Turbulence in accretion discs: the roles of the vertical shear (VSI) and spiral wave (SWI) instabilities

Richard Nelson

Queen Mary, University of London

Collaborators: Oliver Gressel (NBIA, Copenhagen), Orkan Umurhan (NASA-AMES), Samuel Richard (QMUL), Jaehan Bae (Michigan), Lee Hartmann (Michigan)

Queen Mary University of London

Hydrodynamic stability in a disc – i.e. without a magnetic field

Quasi-keplerian discs with Ω=Ω(R) stable according to Rayleigh criterion

$$\frac{\mathrm{d}j^2}{\mathrm{d}r} > 0$$

Compressible adiabatic disc gas with Ω=Ω(R,Z) stable when Solberg-Hoiland criteria are satisfied

$$\frac{1}{R^3}\frac{\partial j^2}{\partial R} + \frac{1}{\rho C_p}\left(\left|\frac{\partial P}{\partial R}\right|\frac{\partial S}{\partial R} + \left|\frac{\partial P}{\partial Z}\right|\frac{\partial S}{\partial Z}\right) > 0$$

$$\frac{\partial j^2}{\partial R}\frac{\partial S}{\partial Z} - \frac{\partial j^2}{\partial Z}\frac{\partial S}{\partial R} > 0.$$

Typically, protoplanetary disc models have stable radial and vertical entropy gradients
-> dynamically stable according to Solberg-Hoiland criteria

Hydrodynamic stability in a disc

Rotating fluid in which thermal diffusion is much more rapid than viscous diffusion is unstable to Goldreich-Schubert-Fricke instability for perturbation modes that satisfy

$$\frac{\partial j^2}{\partial R} - \frac{k_R}{k_Z}\frac{\partial j^2}{\partial Z} < 0.$$

Goldreich & Schubert (1967), Fricke (1968), Urpin & Brandenburg (1998), Urpin (2003), Arlt & Urpin (2004), Nelson, Gressel & Umurhan (2013), Barker & Latter (2015), McNally & Pessah (2015), Lin & Youdin (2015)

$k_R = 2\pi/\lambda_R$ $k_Z = 2\pi/\lambda_Z$

$$\frac{\partial j}{\partial Z} \simeq q\left(\frac{H}{R}\right)\frac{\partial j}{\partial R}$$

➔ for thin disc with radial power-law T profile with index q

Expect unstable modes in thin accretion discs to have $k_R / k_Z \approx R / H$

i.e. radial wavelengths smaller than vertical wavelengths by factor H / R

Disc models and simulations

2D axisymmetric and 3D disc models run with NIRVANA and NIRVANA-III

Density, temperature and angular velocity profiles

$$T(R) = T_0 \left(\frac{R}{R_0}\right)^q$$

$$\rho_{\rm mid}(R) = \rho_0 \left(\frac{R}{R_0}\right)^p$$

$$\rho(R,Z) = \rho_0 \left(\frac{R}{R_0}\right)^p \exp\left(\frac{GM}{c_s^2}\left[\frac{1}{\sqrt{R^2+Z^2}} - \frac{1}{R}\right]\right),$$

$$\Omega(R,Z) = \Omega_K \left[(p+q)\left(\frac{H}{R}\right)^2 + (1+q) - \frac{qR}{\sqrt{R^2+Z^2}}\right]^{1/2}$$

Thermal evolution: Isothermal, adiabatic or Newtonian cooling:

$$\frac{{\rm d}T}{{\rm d}t} = -\frac{(T-T_0)}{\tau_{\rm relax}}$$

See Nelson, Gressel & Umurhan (2013) for details

2D simulations with and without thermal relaxation

Locally isothermal model

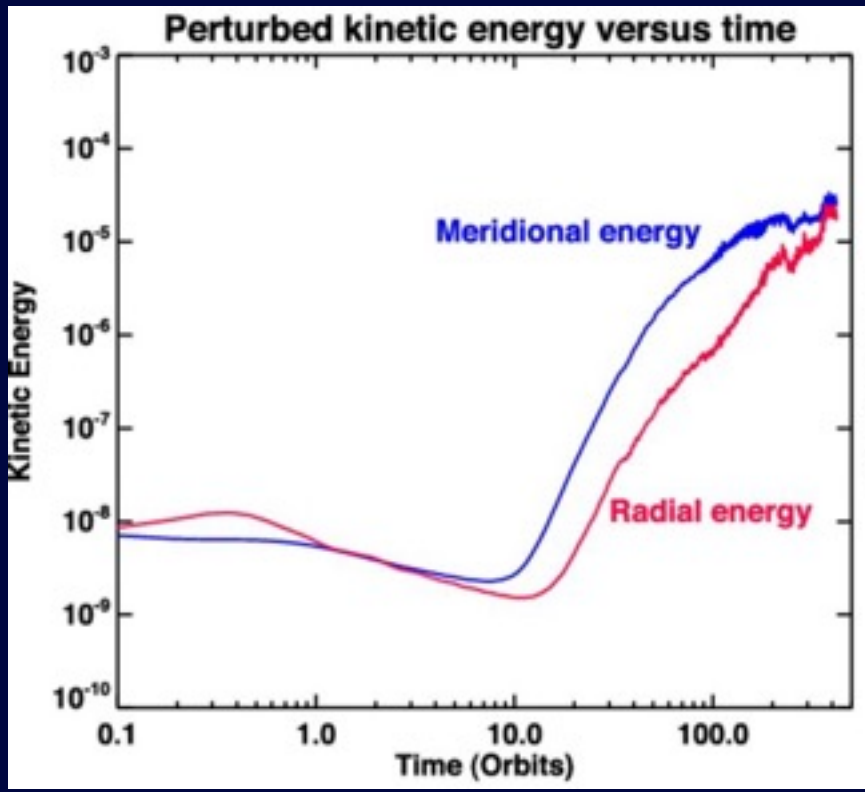

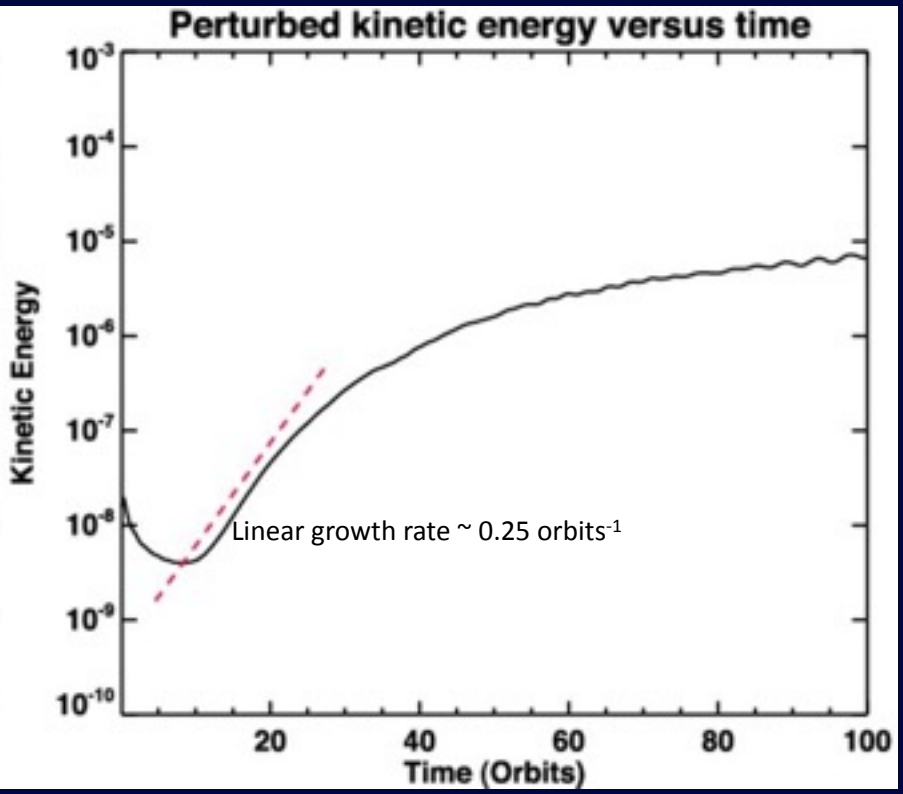

$$T(R) = T_0 \left(\frac{R}{R_0}\right)^q$$

q=-1

$$\rho_{\rm mid}(R) = \rho_0 \left(\frac{R}{R_0}\right)^p$$

p=-1.5

$$e_\theta = \frac{1}{2}\int_V \rho v_\theta^2 dV, \quad e_r = \frac{1}{2}\int_V \rho v_r^2 dV.$$

Numerical set-up

N_R x N_ϑ = (1328 x 1000)

±5 vertical scale heights

Reflecting B.C.s

Seed noise $\delta v = 0.01\ c_s$

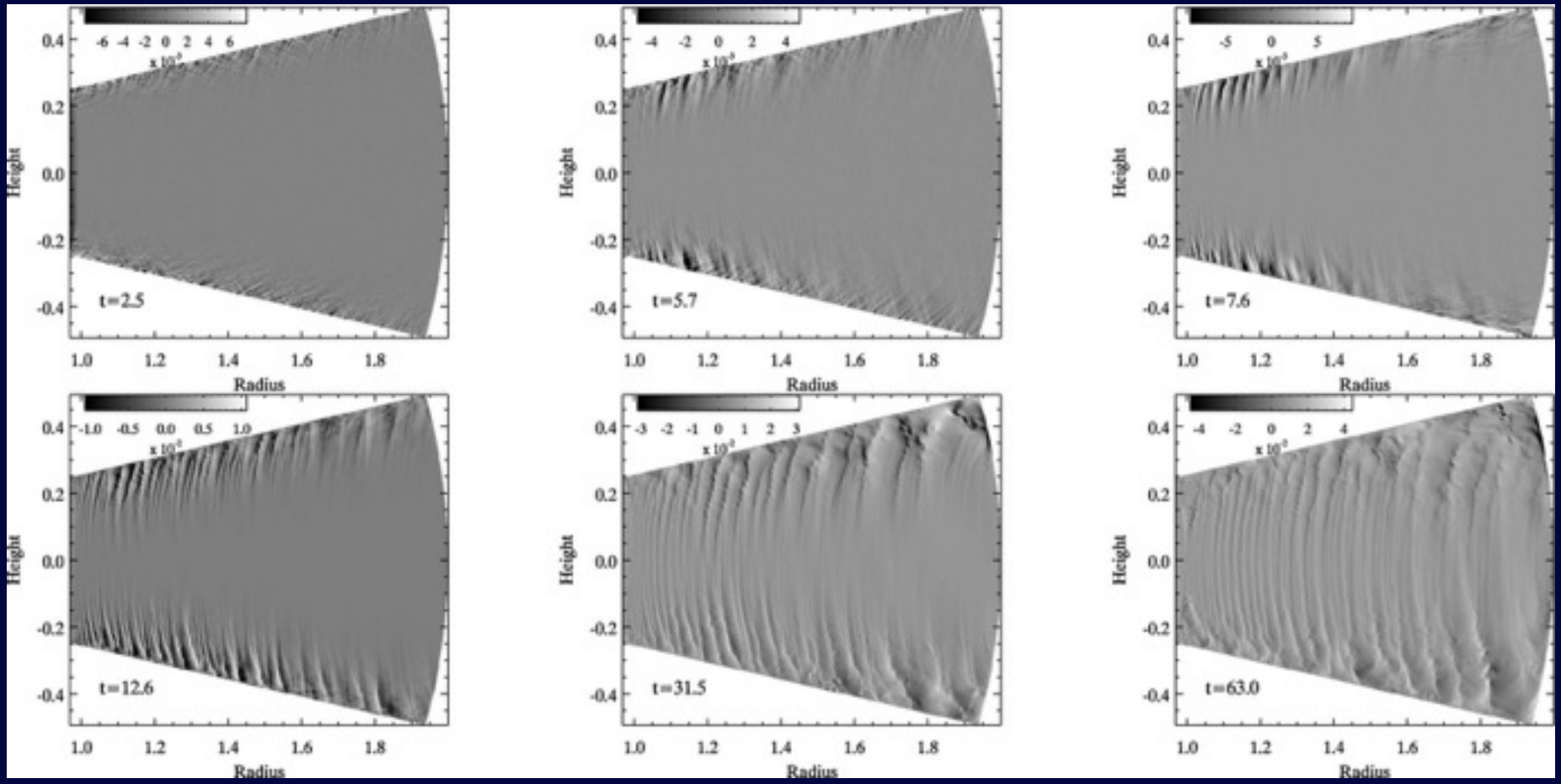

Numerical set-up

N_R x N_ϑ = (1328 x 1000)

±5 vertical scale heights

Reflecting B.C.s

Seed noise $\delta v = 0.01\ c_s$

Vertical velocity perturbations (linear grey-scale)

Note $k_R >> k_Z$

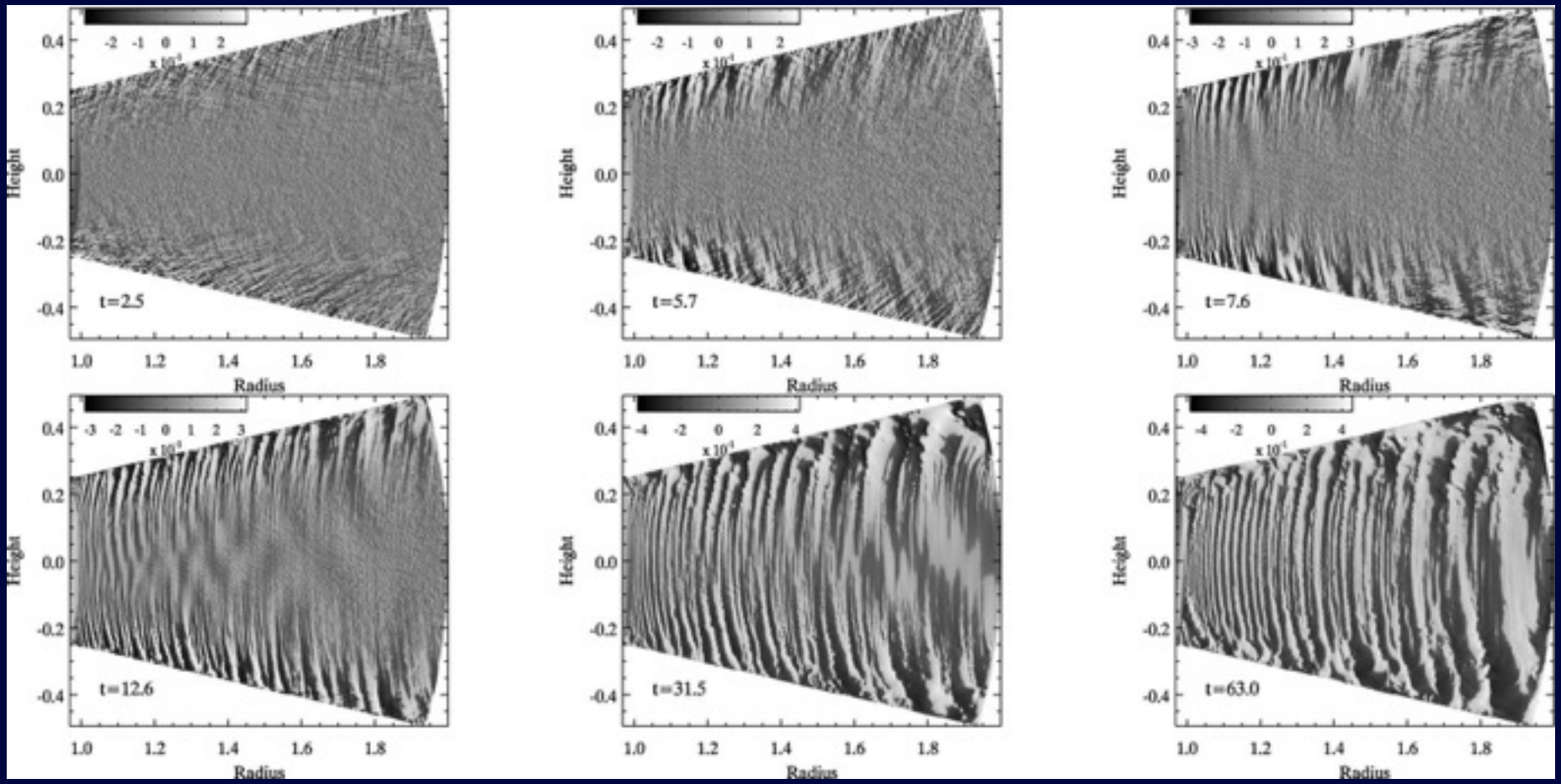

Vertical velocity perturbations (stretched grey-scale)

Note $k_R >> k_Z$

Vertical velocity perturbations

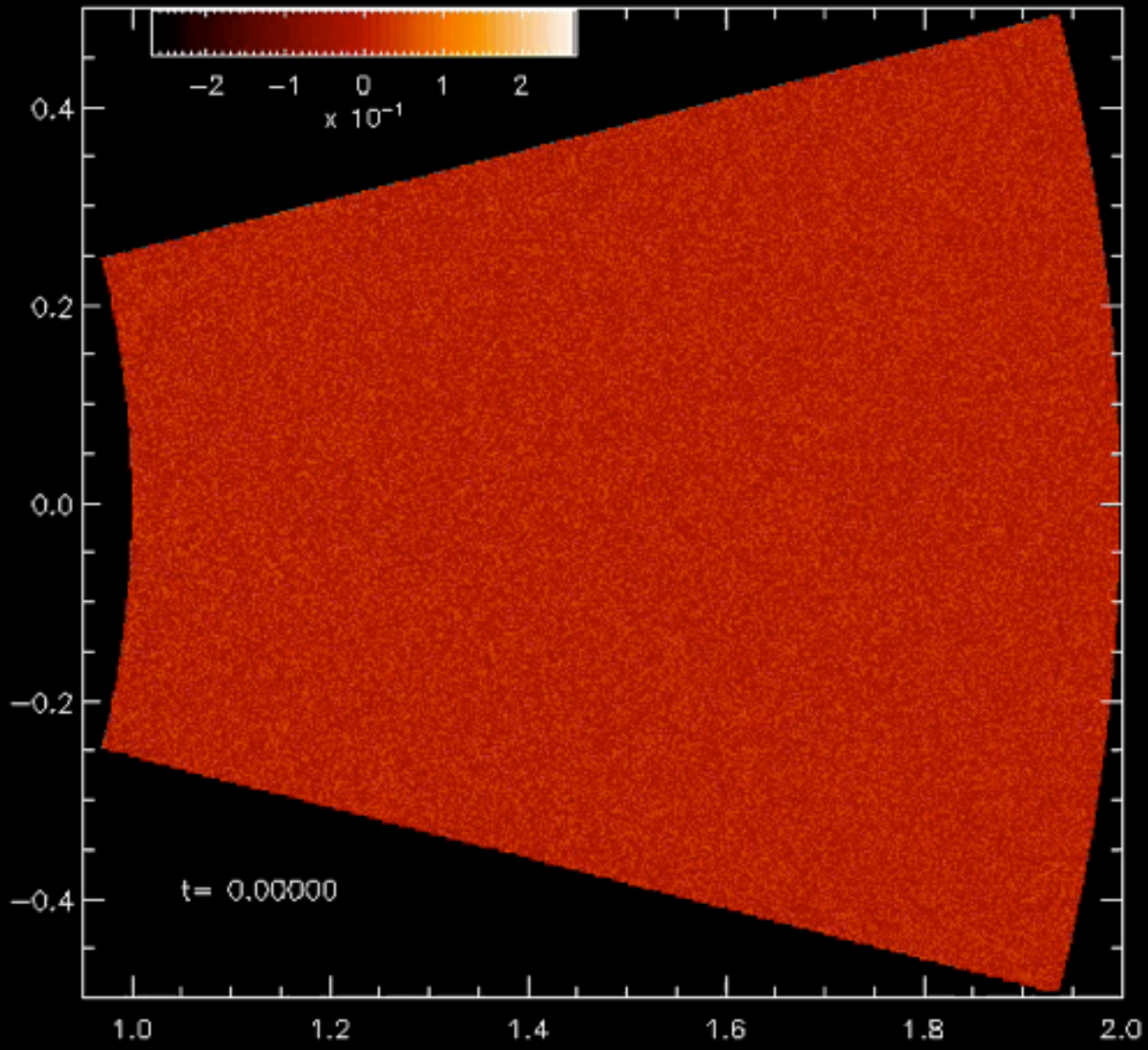

Vertical velocity perturbations

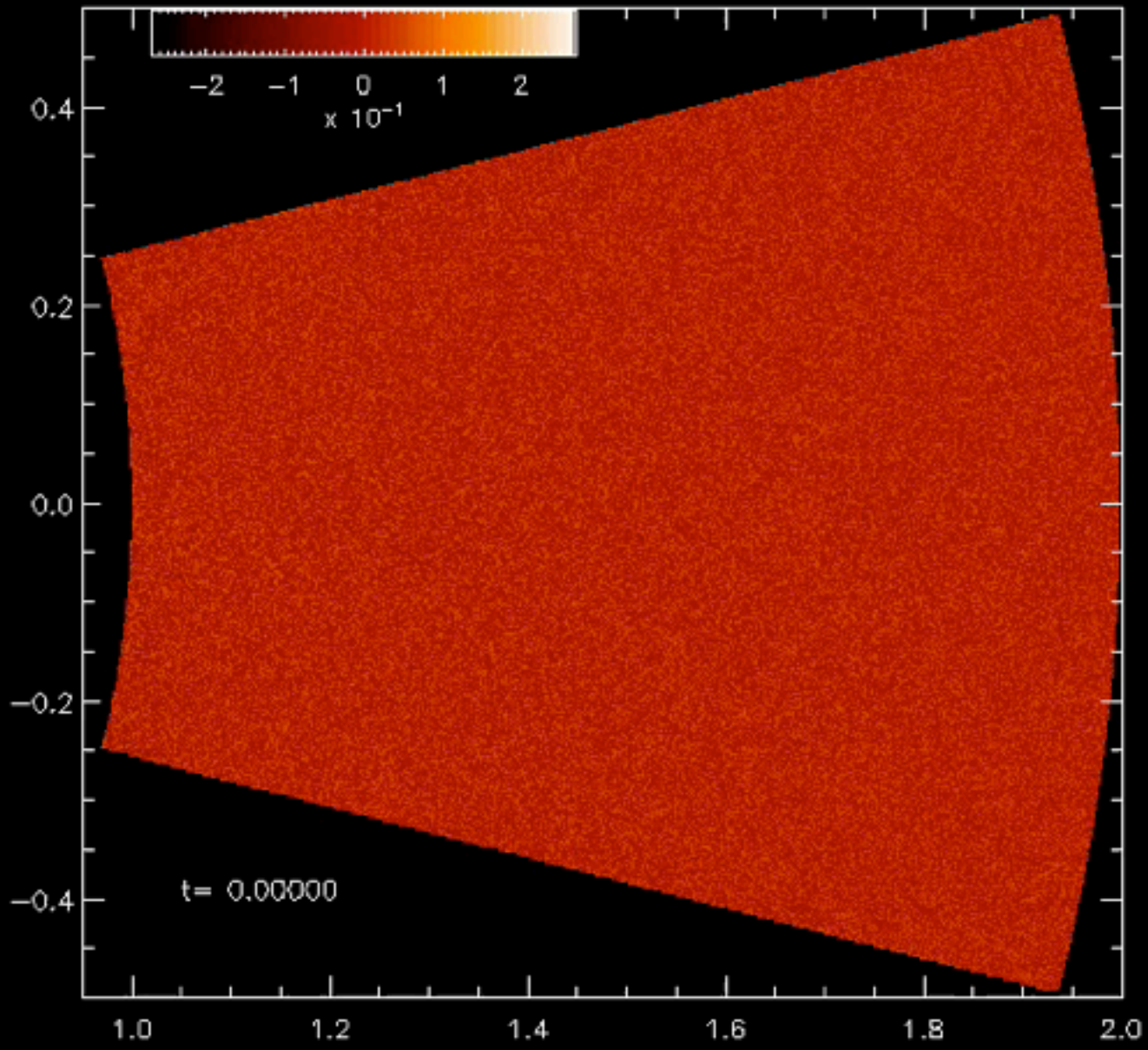

Vertical velocity perturbations

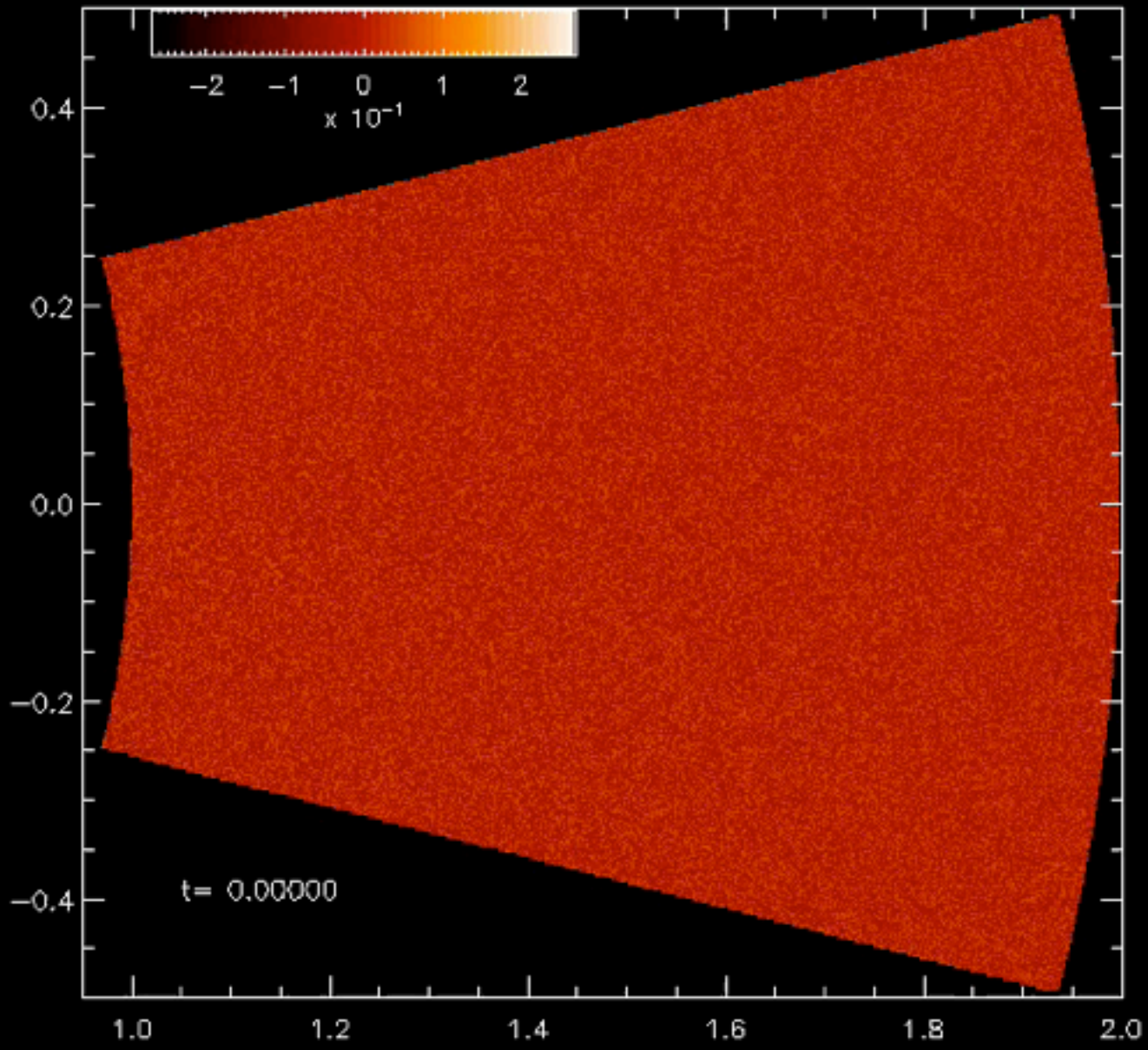

Evolution as function of radial temperature profile: $T \sim R^q$

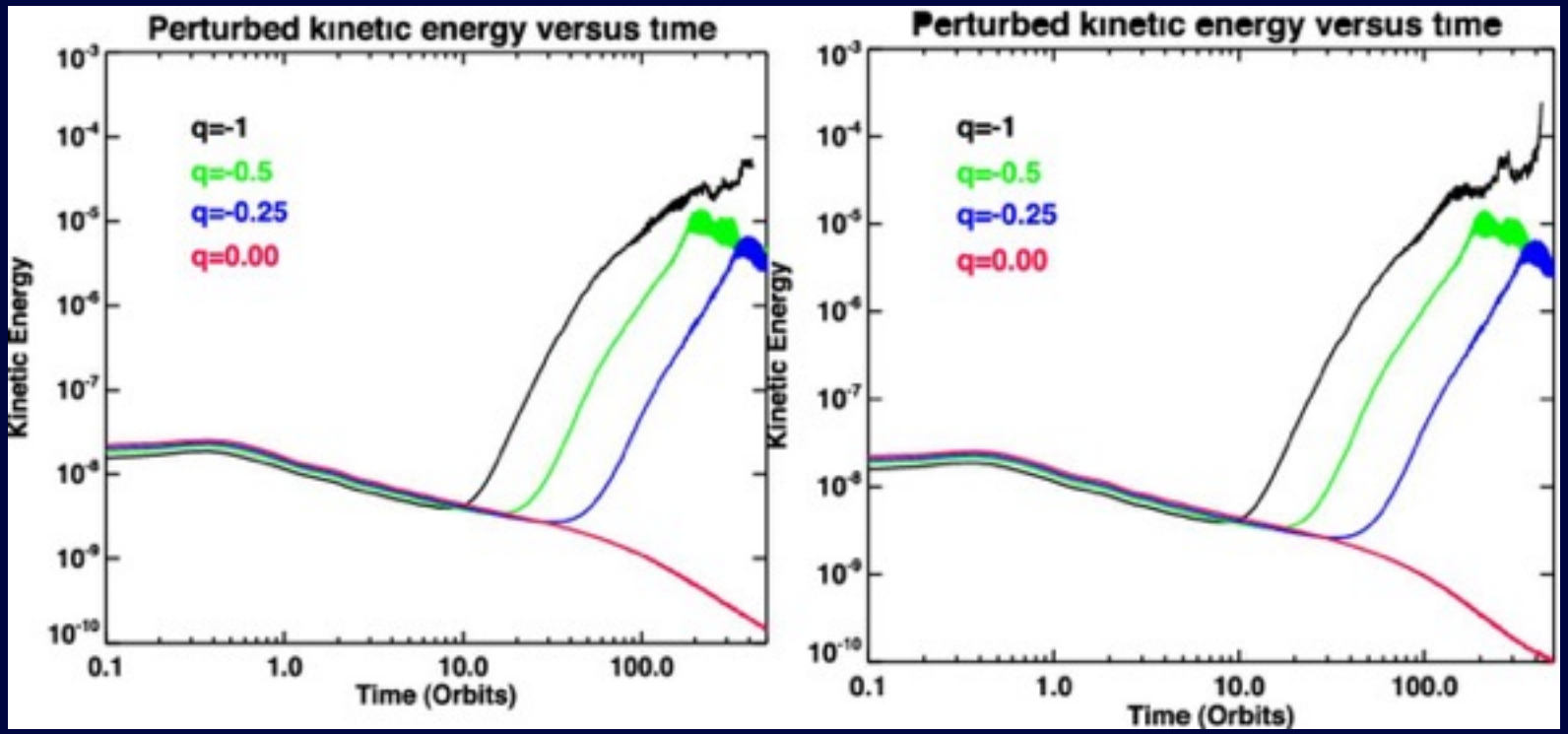

Reflecting boundary conditions

Outflow boundary conditions

Clearly require radial temperature gradient and associated vertical shear for instability

Evolution as function of viscosity

Simulations with constant kinematic viscosity show that instability is damped for $\nu \geq 10^{-6}$
➔ corresponds to $\alpha \geq 4 \times 10^{-4}$

Global simulations of discs with fully-developed MRI turbulence with $\alpha \sim 10^{-3}$ do not show evidence for VSI
(Fromang & Nelson 2006)

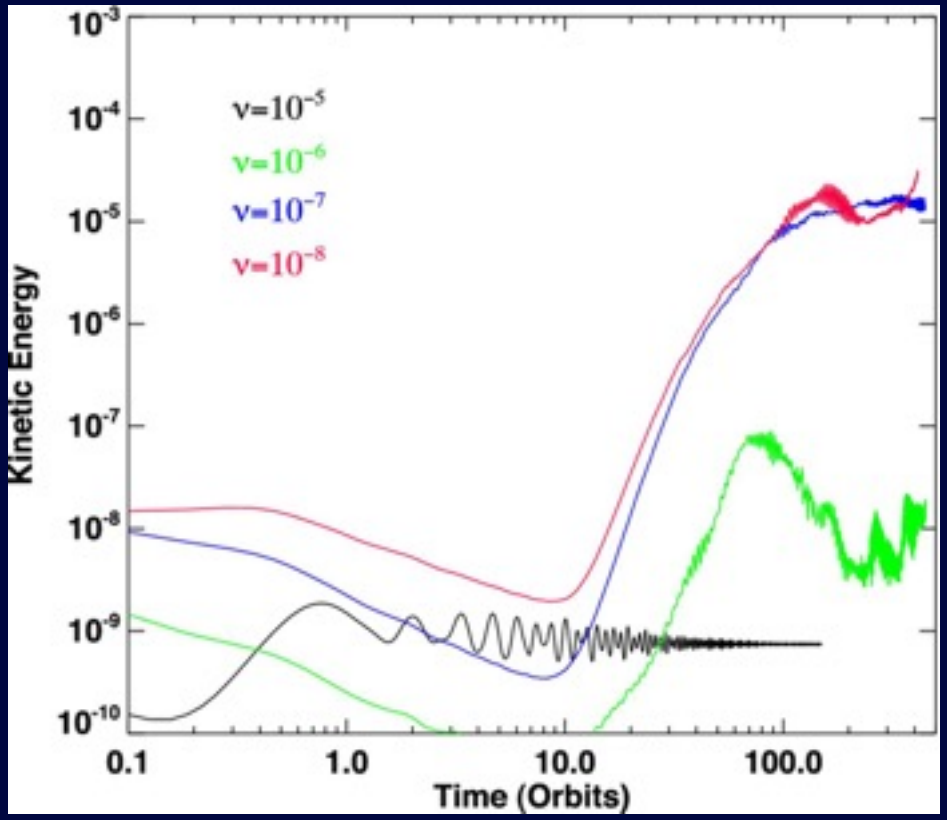

Evolution with thermal relaxation: $T \sim R^{-1}$

$$T(R) = T_0 \left(\frac{R}{R_0}\right)^q$$

q=-1

$$\rho_{\rm mid}(R) = \rho_0 \left(\frac{R}{R_0}\right)^p$$

p=-3/2

$$\frac{dT}{dt} = -\frac{(T - T_0)}{\tau_{\rm relax}}$$

Require short cooling times to overcome stabilizing influence of entropy gradients for these discs

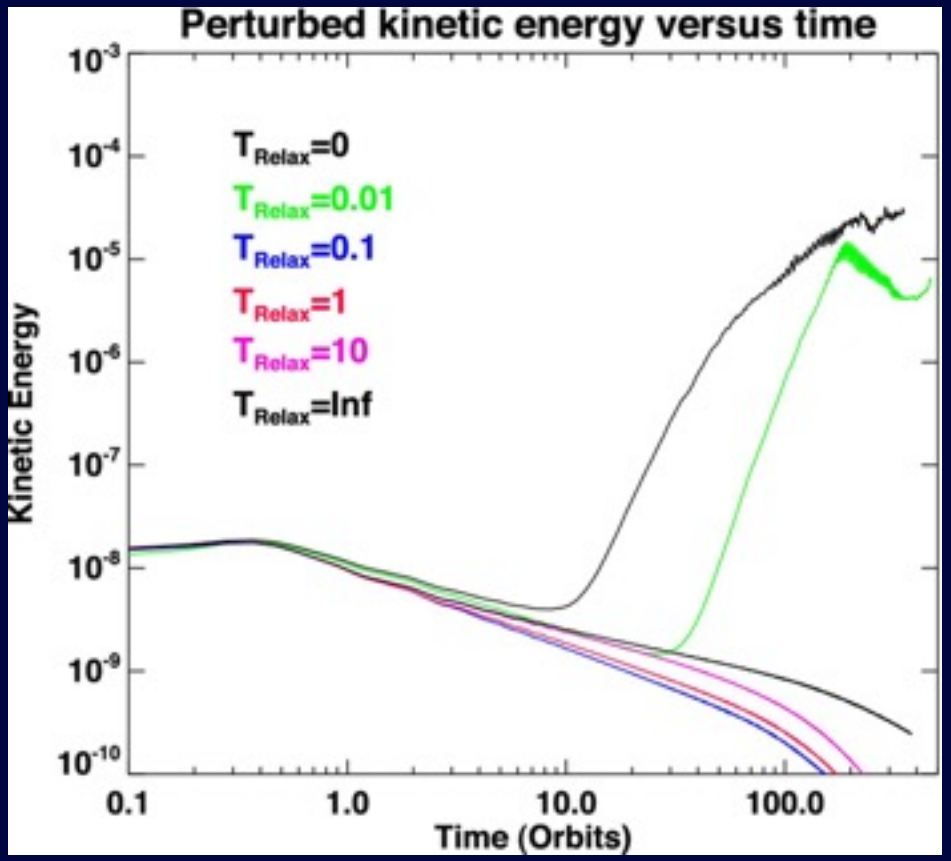

A 3D locally isothermal simulation

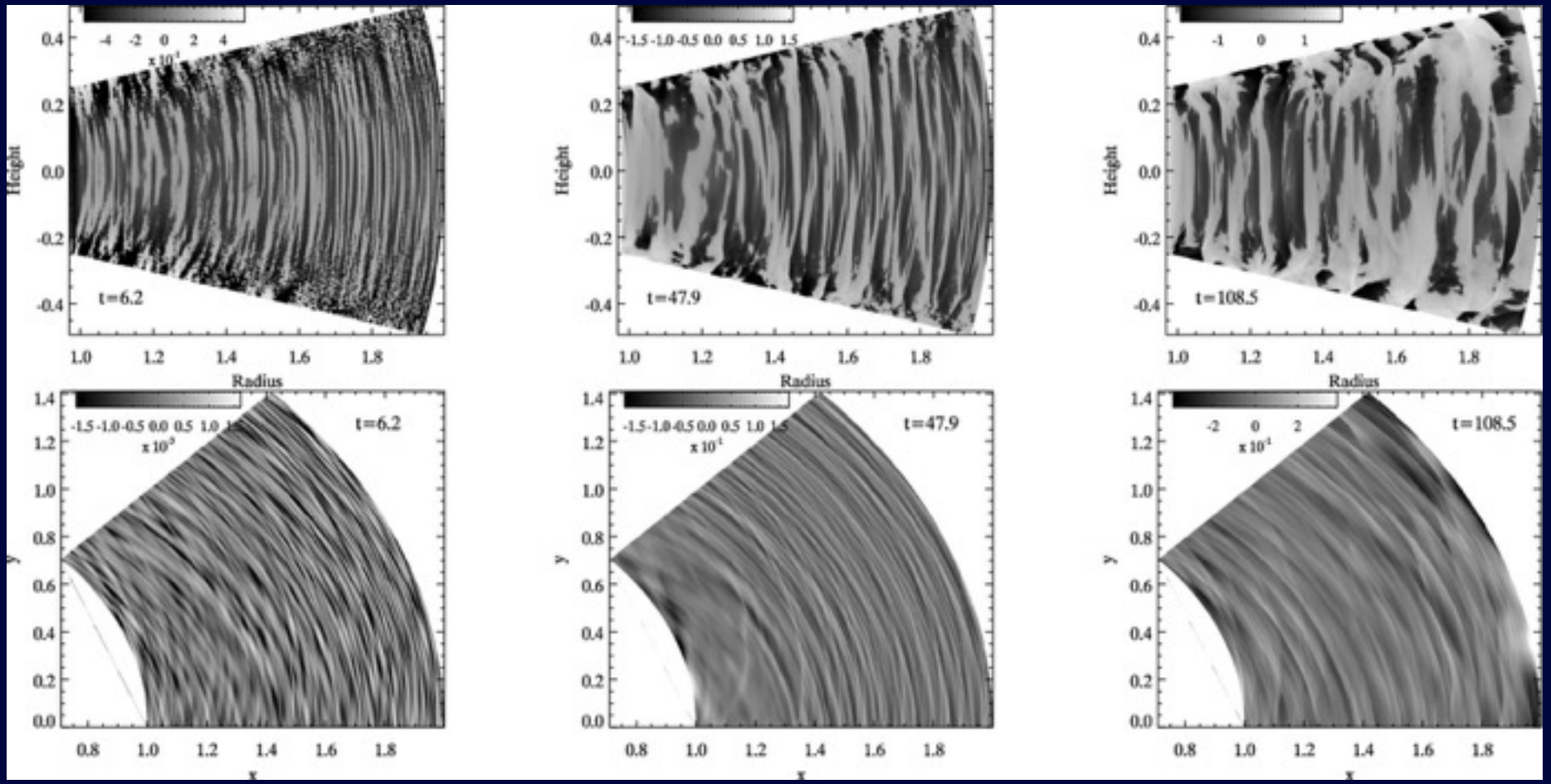

Locally isothermal equation of state

$N_r \times N_\theta \times N_\phi = 1328 \times 1000 \times 300$

in $\pi/4$

Upper panel: vertical velocity perturbations

Lower panel: mid-plane density perturbations

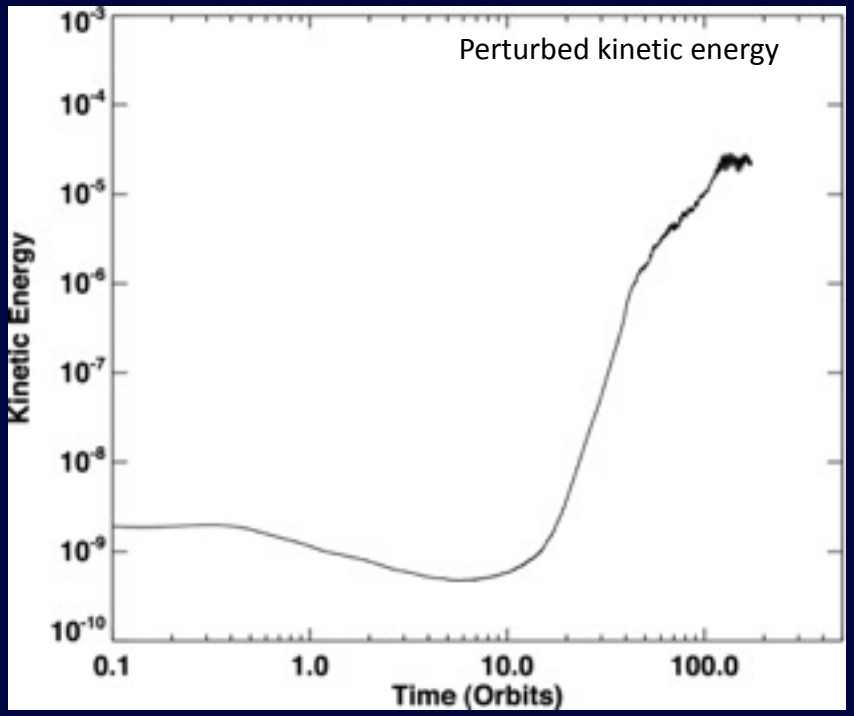

3D simulation show similar growth rate for perturbed energy as 2D runs

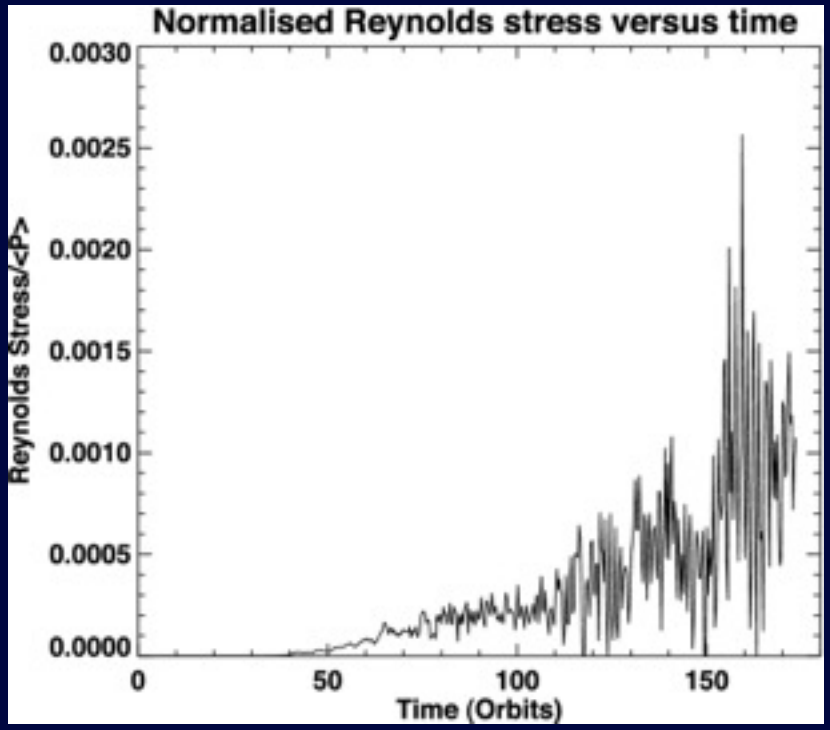

Quasi-turbulence in nonlinear saturated state gives rise to Reynolds stress with effective mean $\alpha \sim 10^{-3}$

Cooling rates in protostellar/protoplanetary discs

Thermal time scale due to radiative diffusion

$$\tau_{\rm Rad} = \frac{\Delta^2}{\mathcal{D}} \qquad \mathcal{D} = \frac{4acT^3}{3\kappa\rho^2 C_{\rm v}}$$

Use MMSN model and temperature structure from Chiang & Goldreich (1997)

$$\frac{\tau_{\rm Rad}}{P_{\rm orb}} = 168 F^2 \kappa \left(\frac{\Delta}{R}\right)^2 \left(\frac{R}{20\,{\rm AU}}\right)^{-53/14}$$

$$\Delta = \lambda_R \simeq \frac{H^2}{R}$$

VSI likely to operate in outer regions (beyond 10 – 20 AU) of protoplanetary discs

$$\frac{\tau_{\rm Rad}}{P_{\rm orb}} = 0.015$$ At 10 AU

$$\frac{\tau_{\rm Rad}}{P_{\rm orb}} = 0.001$$ At 20 AU

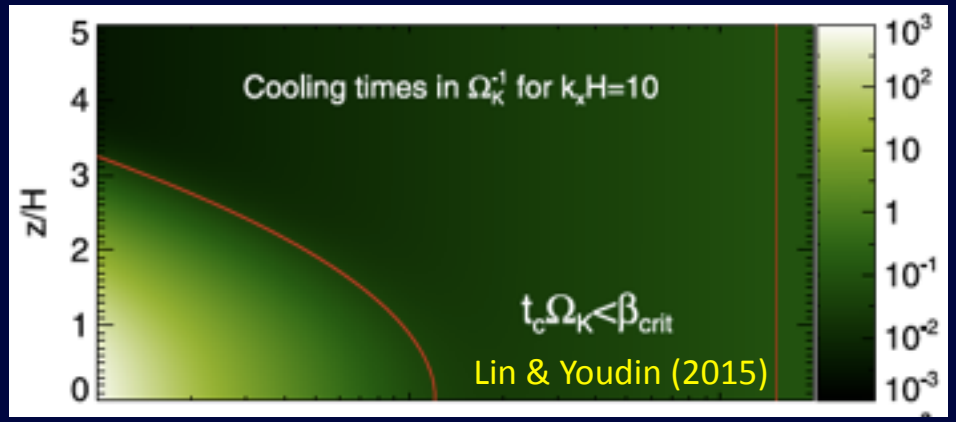

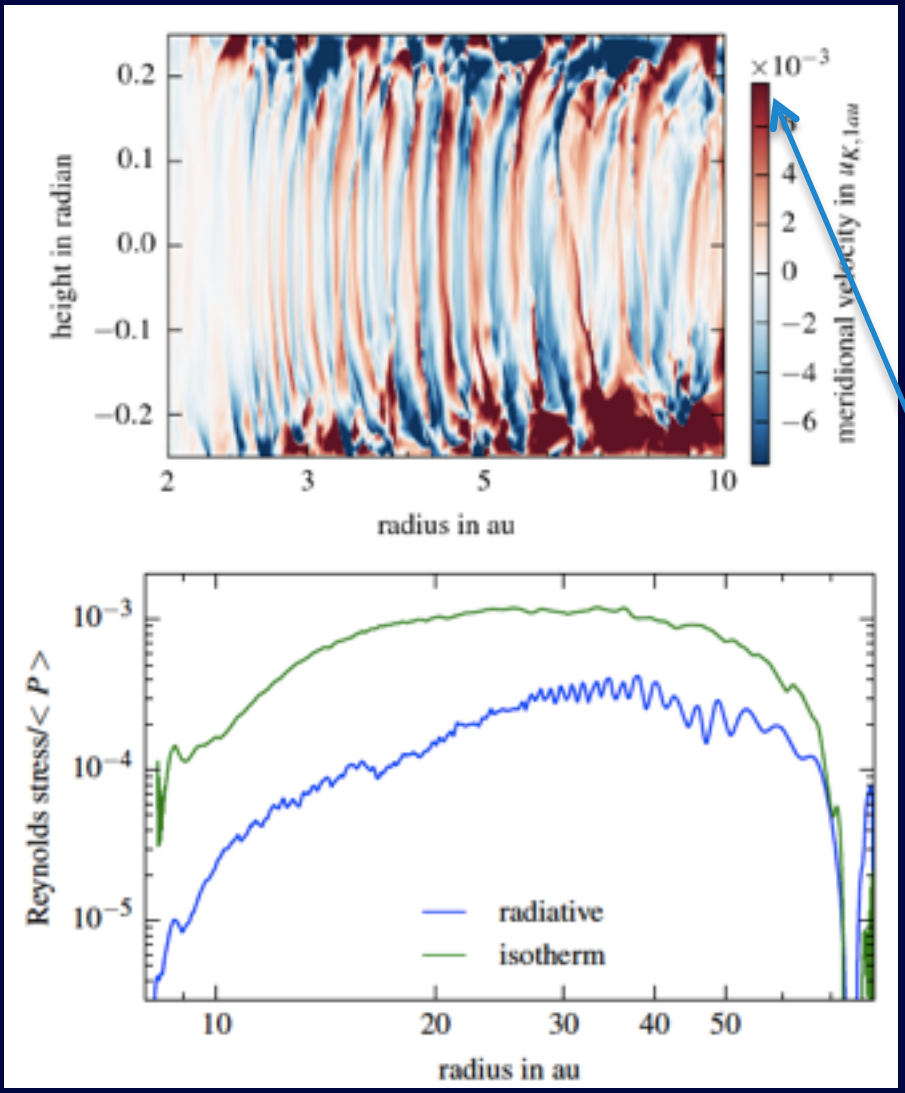

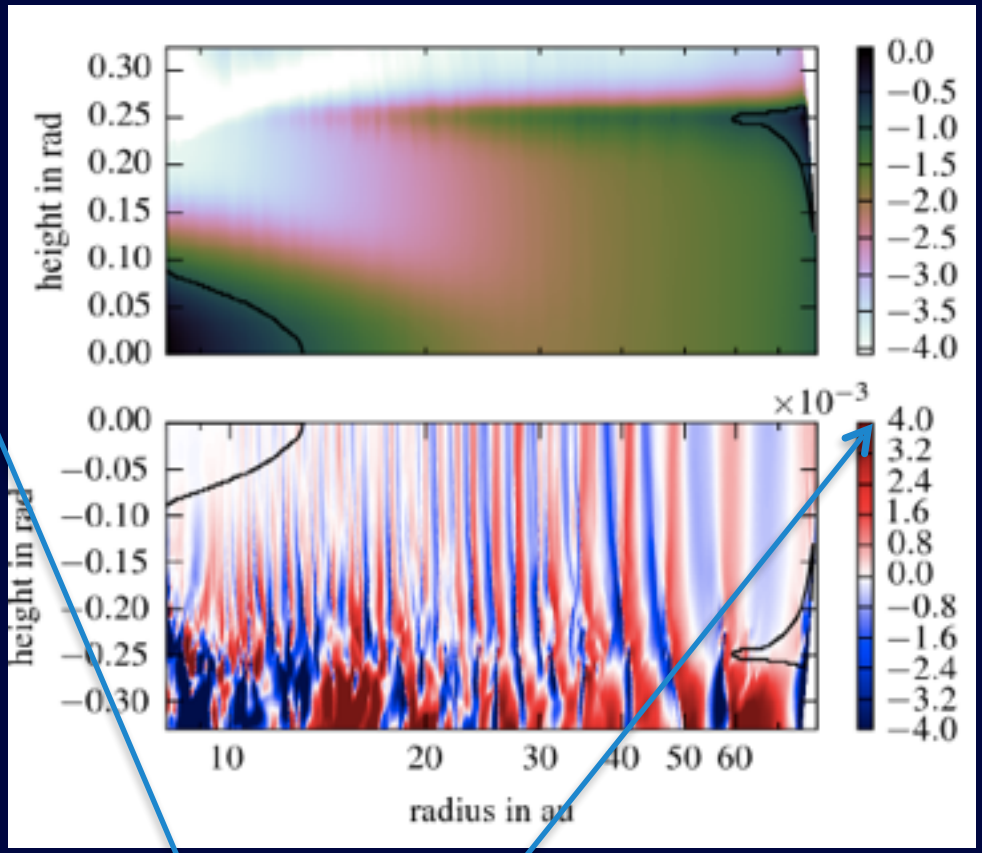

V_z ~ 0.3 x c_s

V_z ~ 0.2 x c_s

VSI induces turbulent velocities v_z ~ 0.2 x c_s near disc surfaces

Stoll & Kley (2016) study VSI for irradiated discs with internal radiation transport using flux limited diffusion - nonlinear state of instability similar to simple models

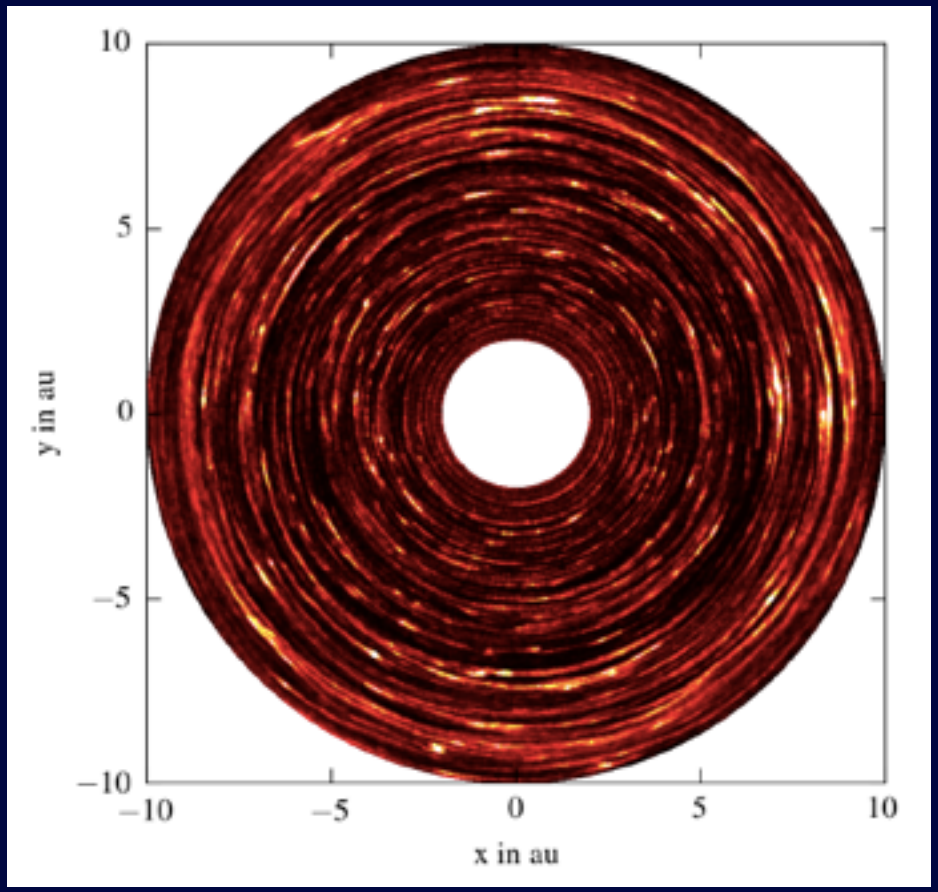

Particle concentration in pressure bumps
(see also Richard, Nelson & Umurhan 2016)

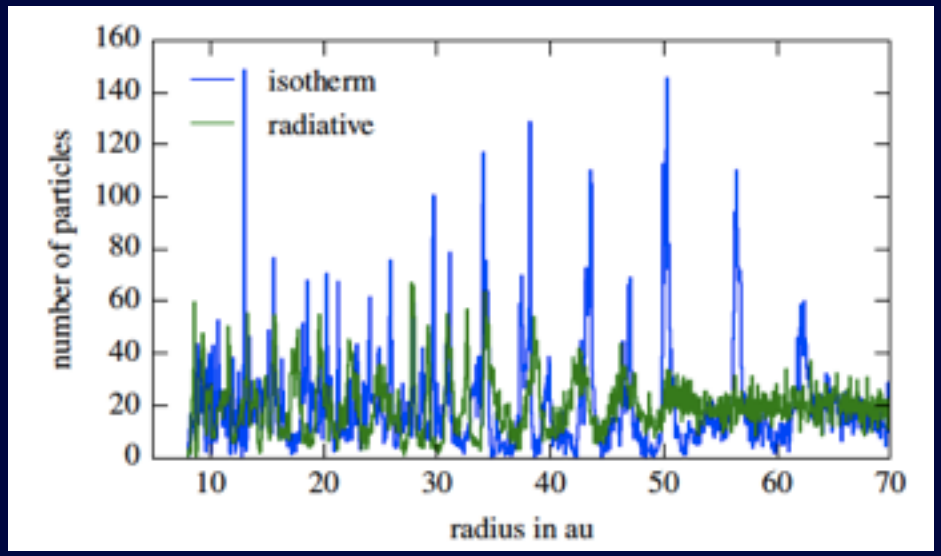

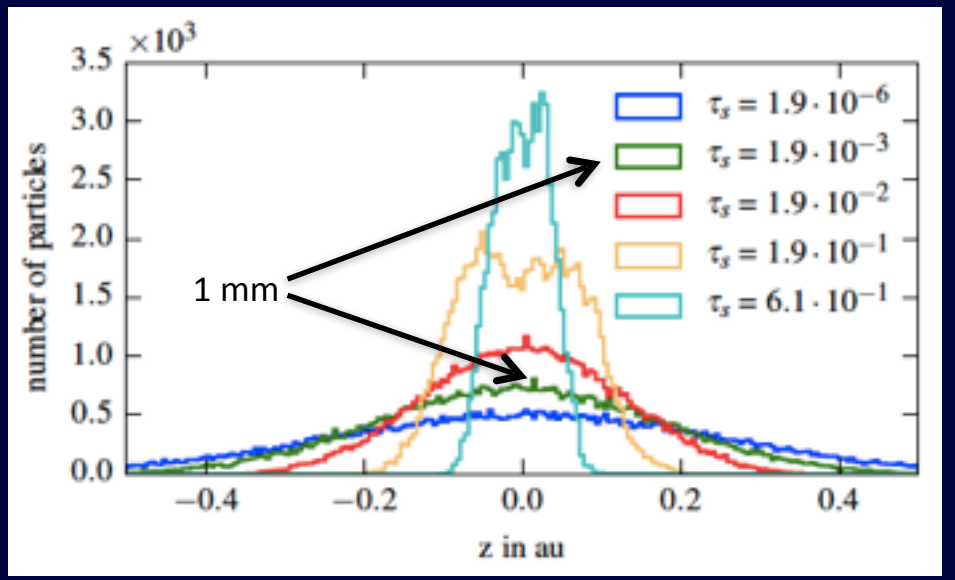

Anisotropic diffusion leads to vertical mixing of dust and pebbles

Spiral Wave Instability

Spiral arms in circumstellar disks

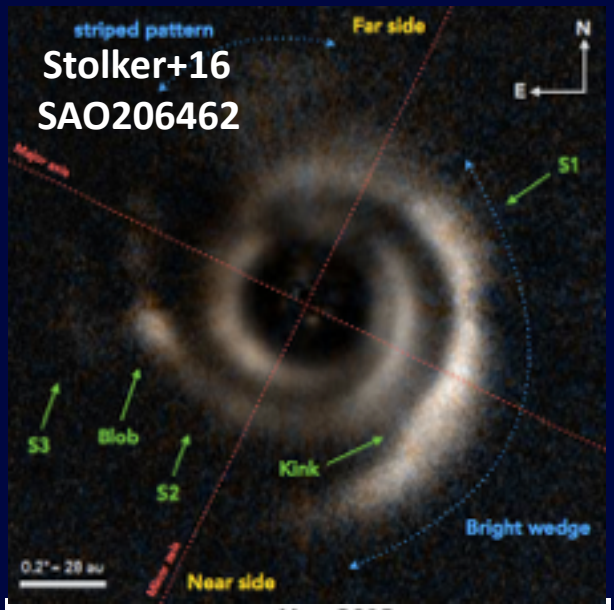

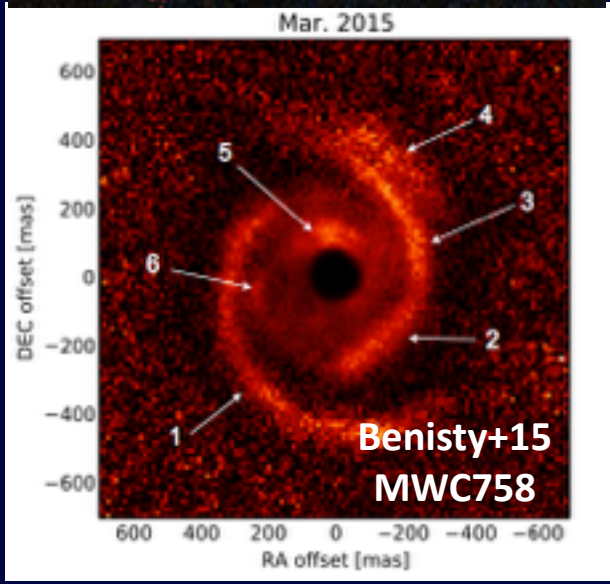

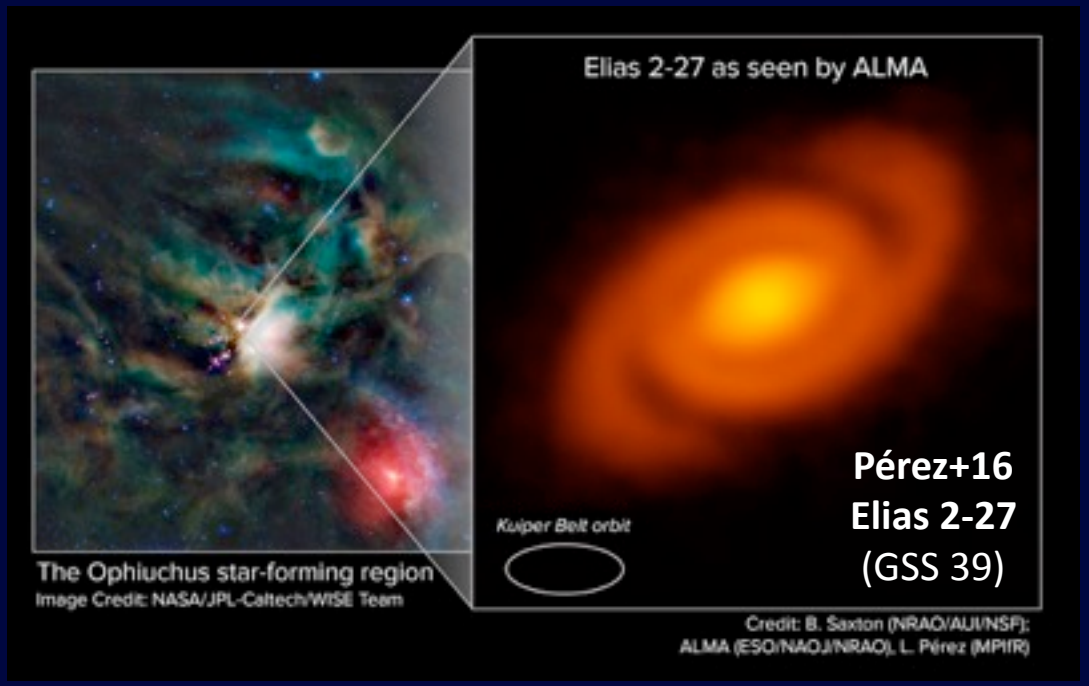

The roles of spiral waves

Transport angular momentum and mass in discs

(e.g. Lynden-Bell & Kalnajs 1972)

The roles of spiral waves

Transport angular momentum and mass in discs
(e.g. Lynden-Bell & Kalnajs 1972)

Heat the disk through PdV work and shock dissipation

The roles of spiral waves

Transport angular momentum and mass in discs
(e.g. Lynden-Bell & Kalnajs 1972)

Heat the disk through PdV work and shock dissipation

Important in a broad variety of contexts related to accretion discs:

- Self-gravitating discs (e.g. Papaloizou & Savonije 1991, Laughlin & Bodenheimer 1994)
  + FU Orionis outbursts (Gammie 1999, Zhu et al 2010, Bae et al. 2013a, 2014)

The roles of spiral waves

Transport angular momentum and mass in discs
(e.g. Lynden-Bell & Kalnajs 1972)

Heat the disk through PdV work and shock dissipation

Important in a broad variety of contexts related to accretion discs:

- Self-gravitating discs (e.g. Papaloizou & Savonije 1991, Laughlin & Bodenheimer 1994)
  + FU Orionis outbursts (Gammie 1999, Zhu et al 2010, Bae et al. 2013a, 2014)

- Close binary systems (Lin & Papaloizou 1979, Sawada et al 1986, Artymowicz & Lubow 1994)

The roles of spiral waves

Transport angular momentum and mass in discs
(e.g. Lynden-Bell & Kalnajs 1972)

Heat the disk through PdV work and shock dissipation

Important in a broad variety of contexts related to accretion discs:

- Self-gravitating discs (e.g. Papaloizou & Savonije 1991, Laughlin & Bodenheimer 1994)
  + FU Orionis outbursts (Gammie 1999, Zhu et al 2010, Bae et al. 2013a, 2014)
- Close binary systems (Lin & Papaloizou 1979, Sawada et al 1986, Artymowicz & Lubow 1994)
- Disc-planet interactions (Goldreich & Tremaine 1980, Bryden et al 1999, Kley 1999)

The roles of spiral waves

Transport angular momentum and mass in discs
(e.g. Lynden-Bell & Kalnajs 1972)

Heat the disk through PdV work and shock dissipation

Important in a broad variety of contexts related to accretion discs:

- Self-gravitating discs (e.g. Papaloizou & Savonije 1991, Laughlin & Bodenheimer 1994)
  + FU Orionis outbursts (Gammie 1999, Zhu et al 2010, Bae et al. 2013a, 2014)
- Close binary systems (Lin & Papaloizou 1979, Sawada et al 1986, Artymowicz & Lubow 1994)
- Disc-planet interactions (Goldreich & Tremaine 1980, Bryden et al 1999, Kley 1999)

But, spiral waves are unstable in 3D -> turbulence (Bae et al. 2016a,b)

Circumstellar disc with external binary companion

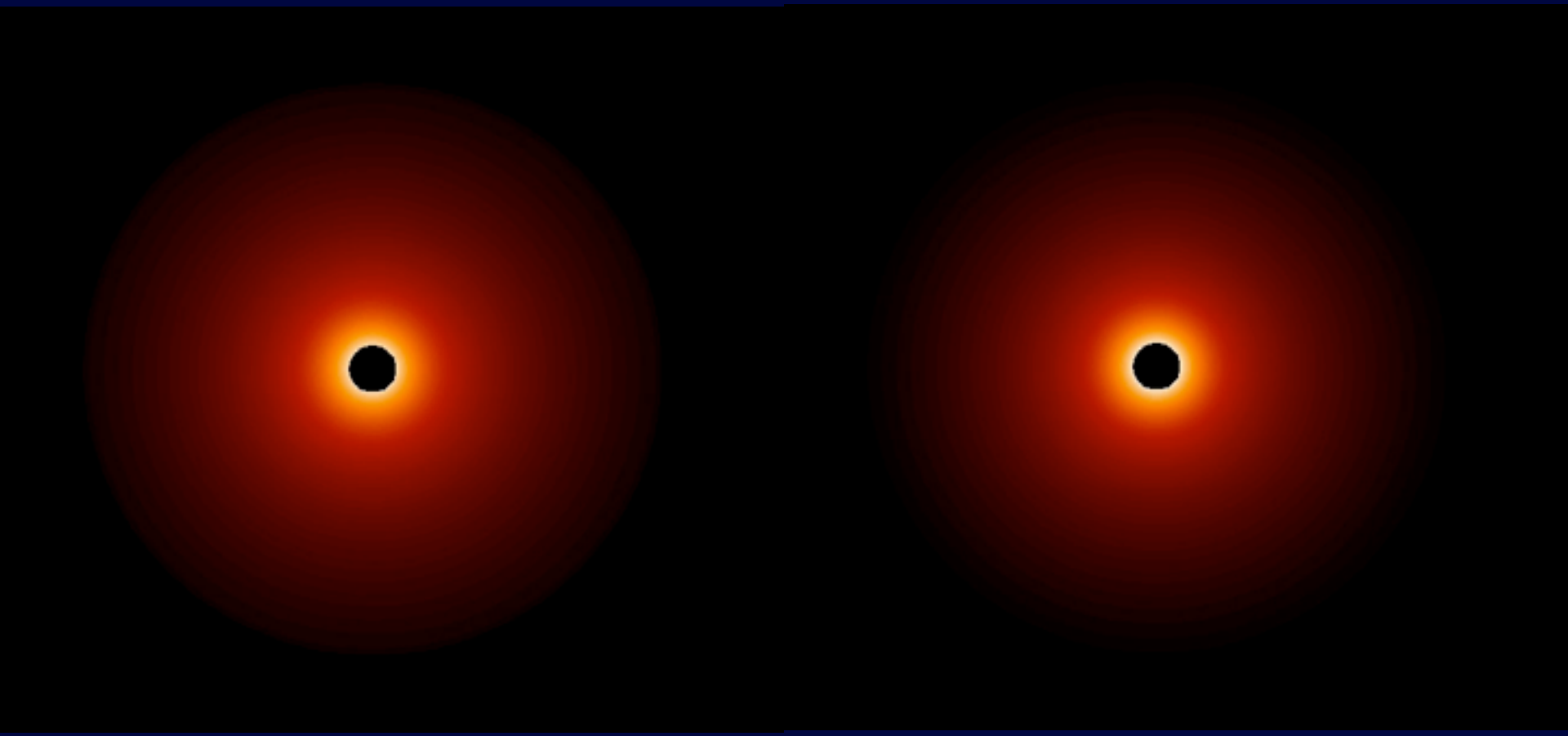

2D

3D

Circumstellar disc with external binary companion

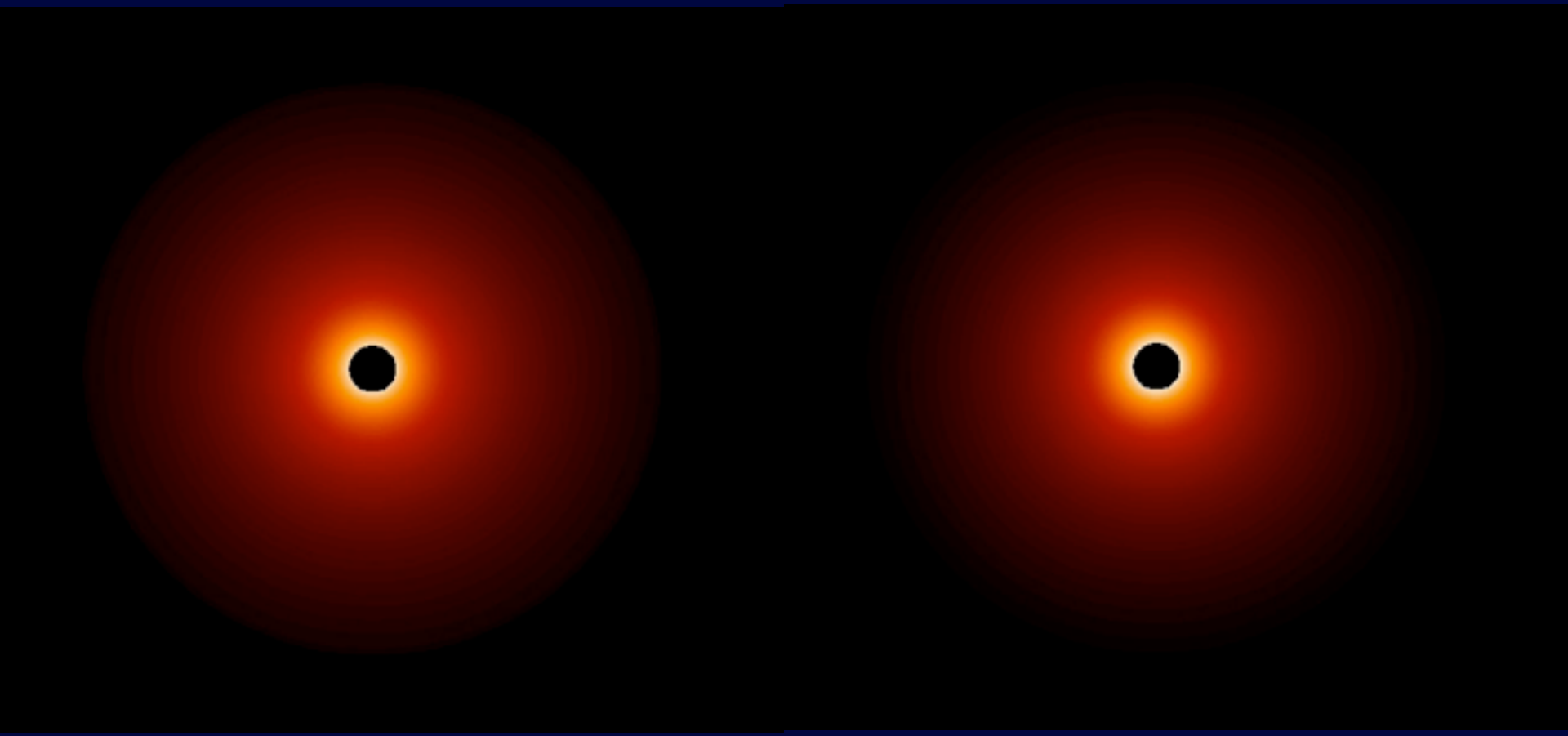

2D

3D

Circumstellar disc with external binary companion

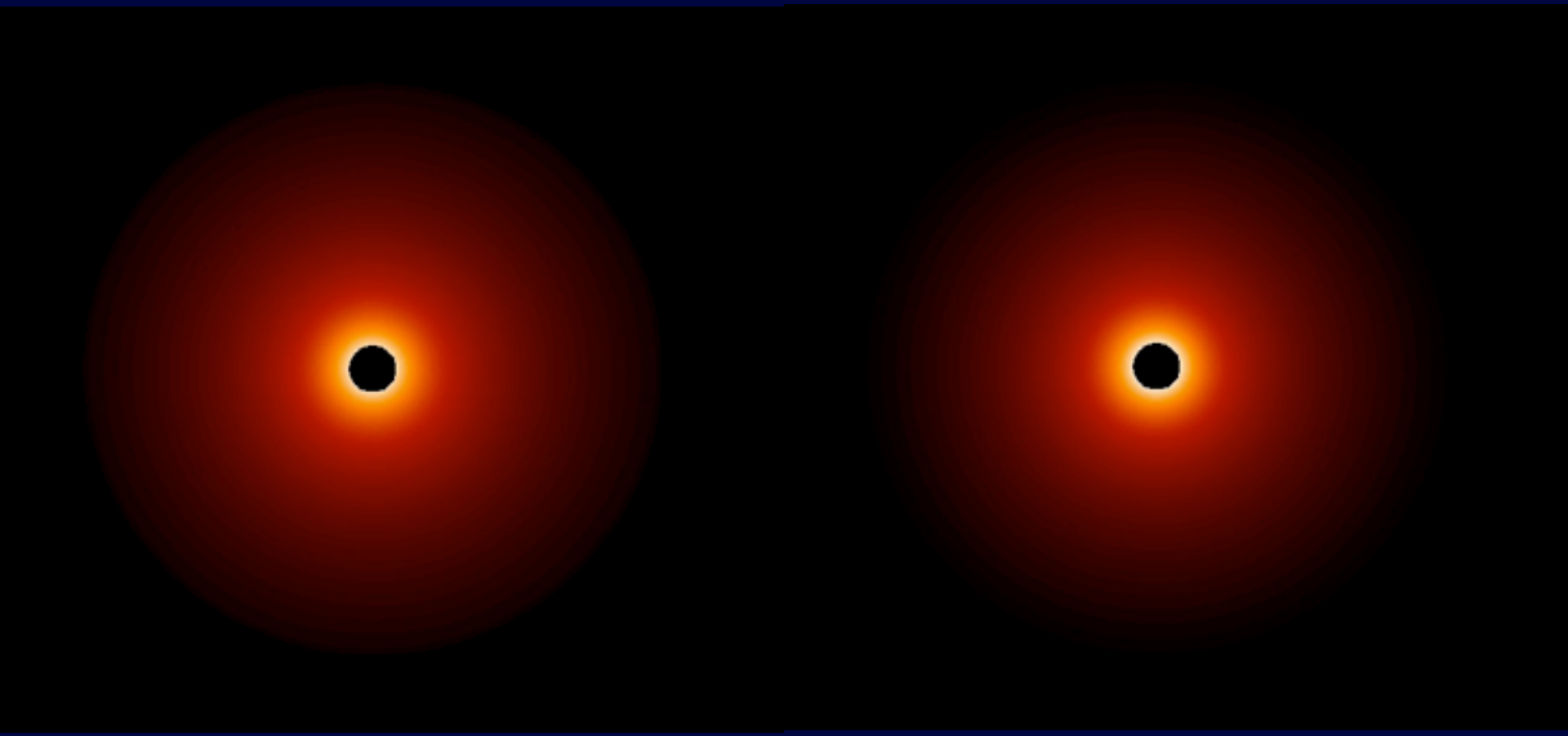

2D

3D

Circumstellar disc with external binary companion

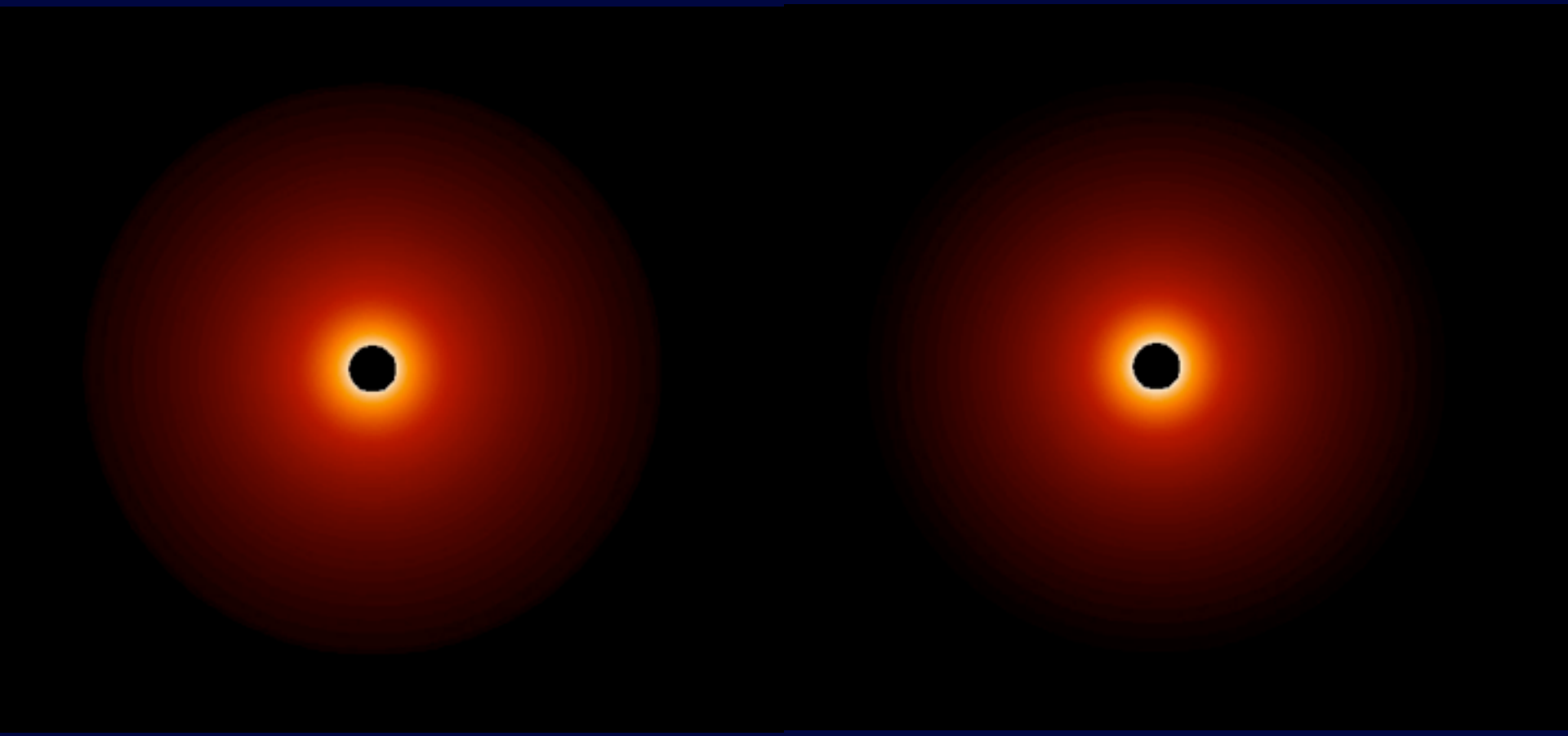

2D

3D

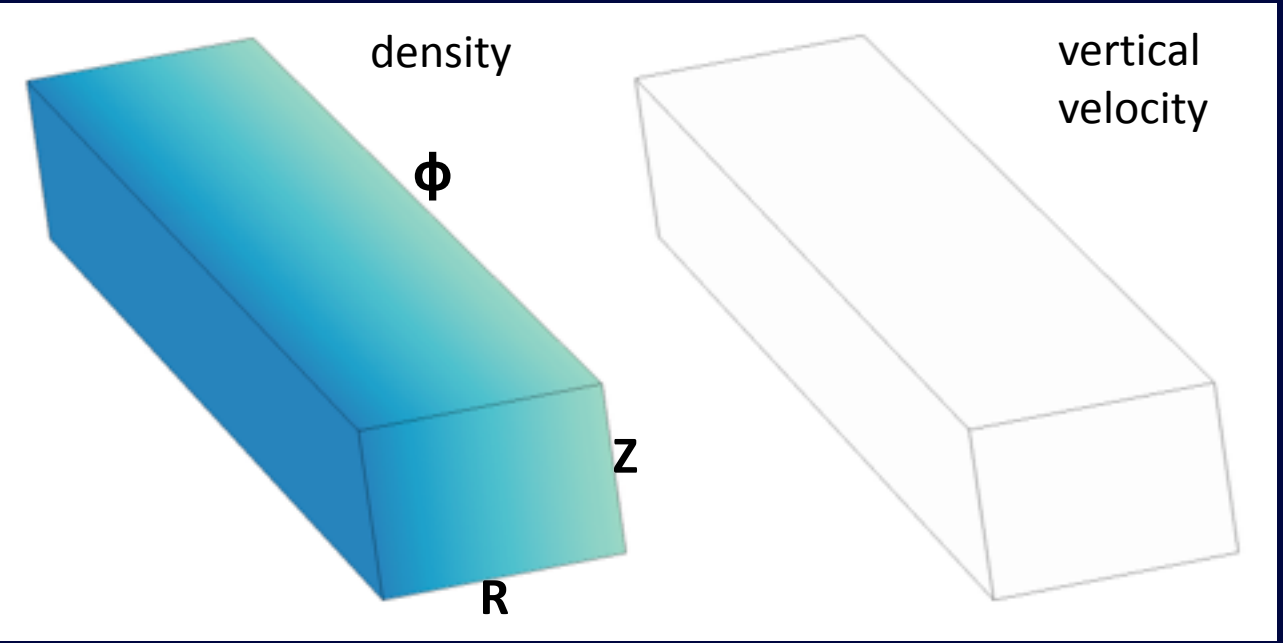

Monochromatic m=2 spiral waves are driven in a local unstratified shearing box

64 grid cells per scale height (cell size ~80,000 km at 1 AU with H/R=0.033)

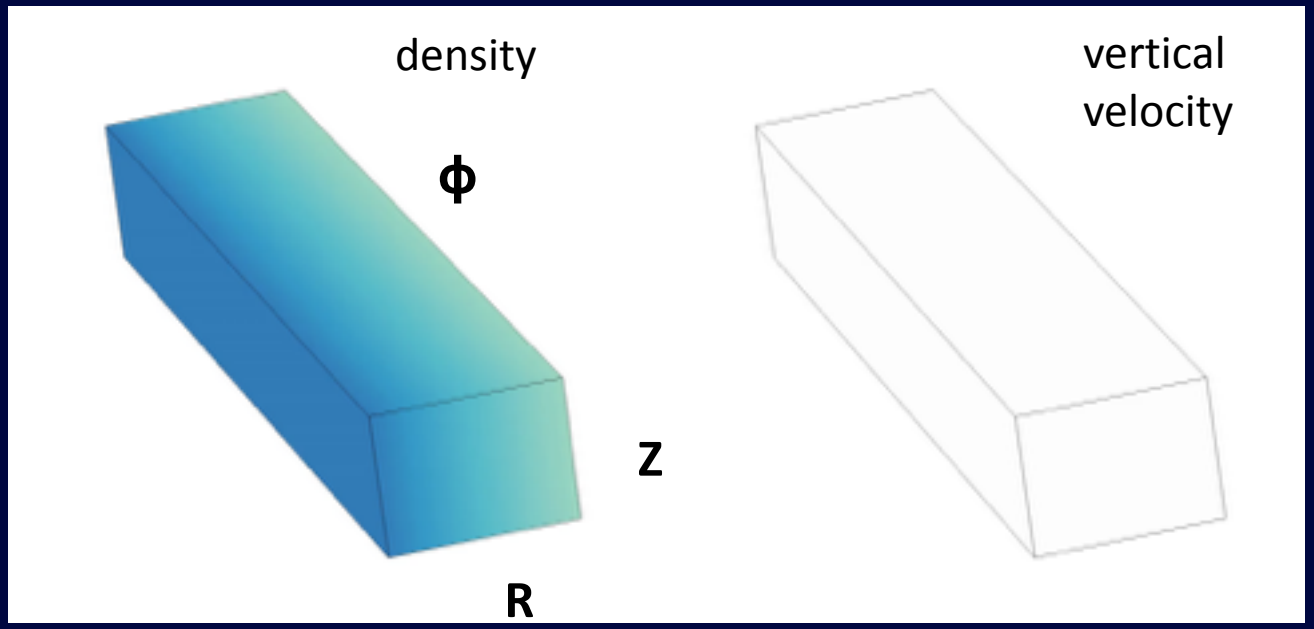

Monochromatic m=2 spiral waves are driven in a local unstratified shearing box

64 grid cells per scale height (cell size ~80,000 km at 1 AU with H/R=0.033)

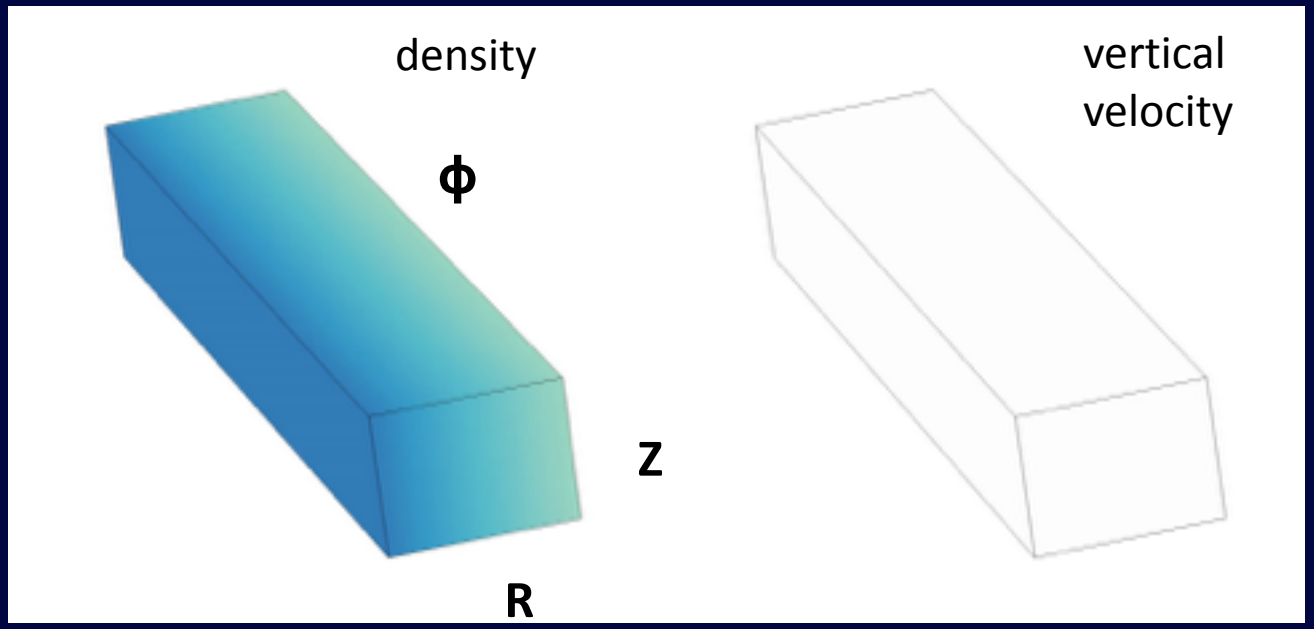

Monochromatic m=2 spiral waves are driven in a local unstratified shearing box

64 grid cells per scale height (cell size ~80,000 km at 1 AU with H/R=0.033)

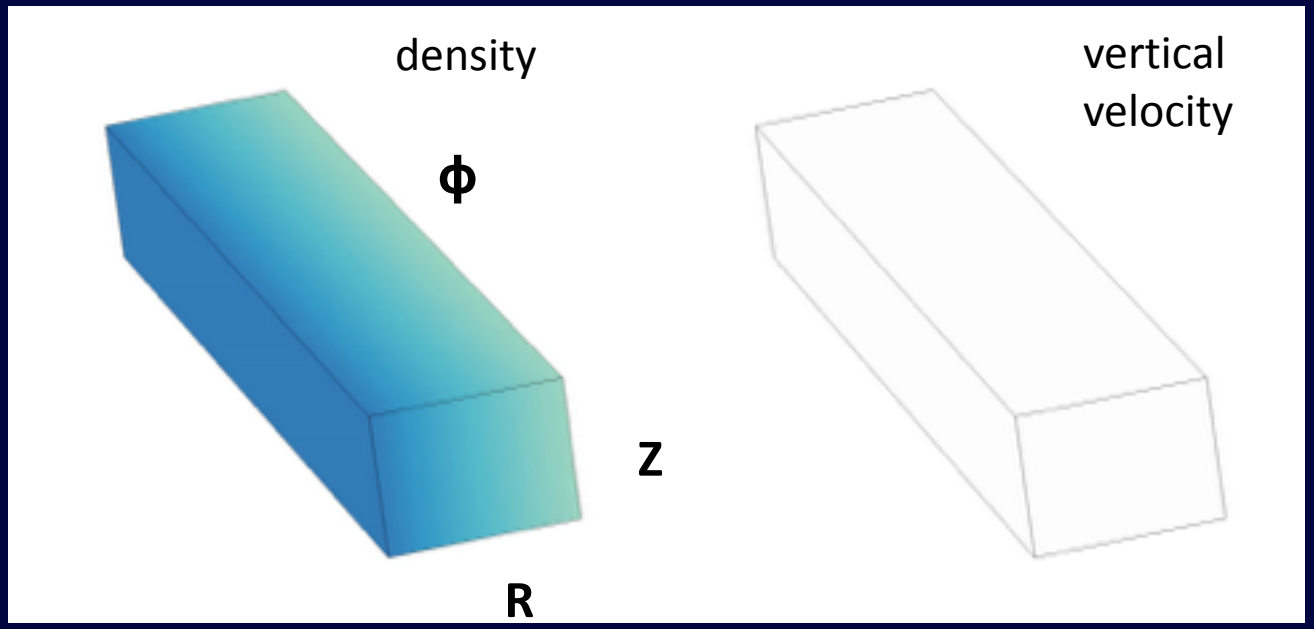

Monochromatic m=2 spiral waves are driven in a local unstratified shearing box

64 grid cells per scale height (cell size ~80,000 km at 1 AU with H/R=0.033)

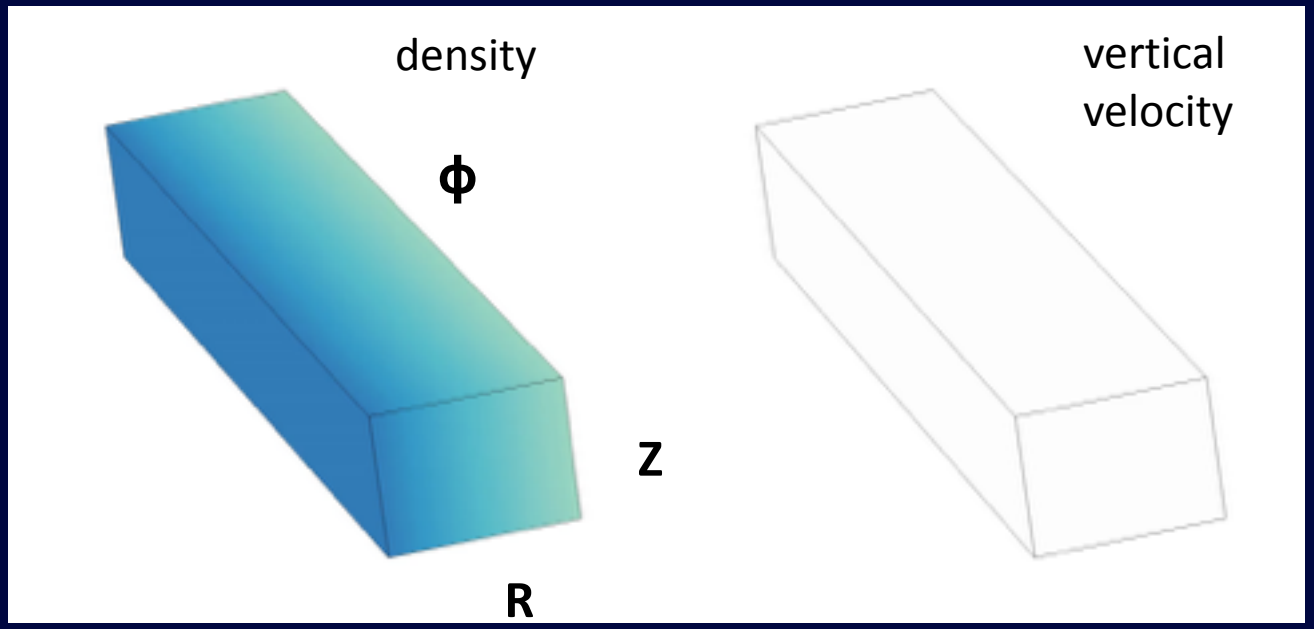

Monochromatic m=2 spiral waves are driven in a local unstratified shearing box

64 grid cells per scale height (cell size ~80,000 km at 1 AU with H/R=0.033)

Origin of the instability

- Pairs of inertial modes amplify as they resonantly couple with and extract energy from the background spiral wave
- Maximum growth rate obtained when $\omega_{i1} + \omega_{i2} = \omega_s$ (Goodman 1993).

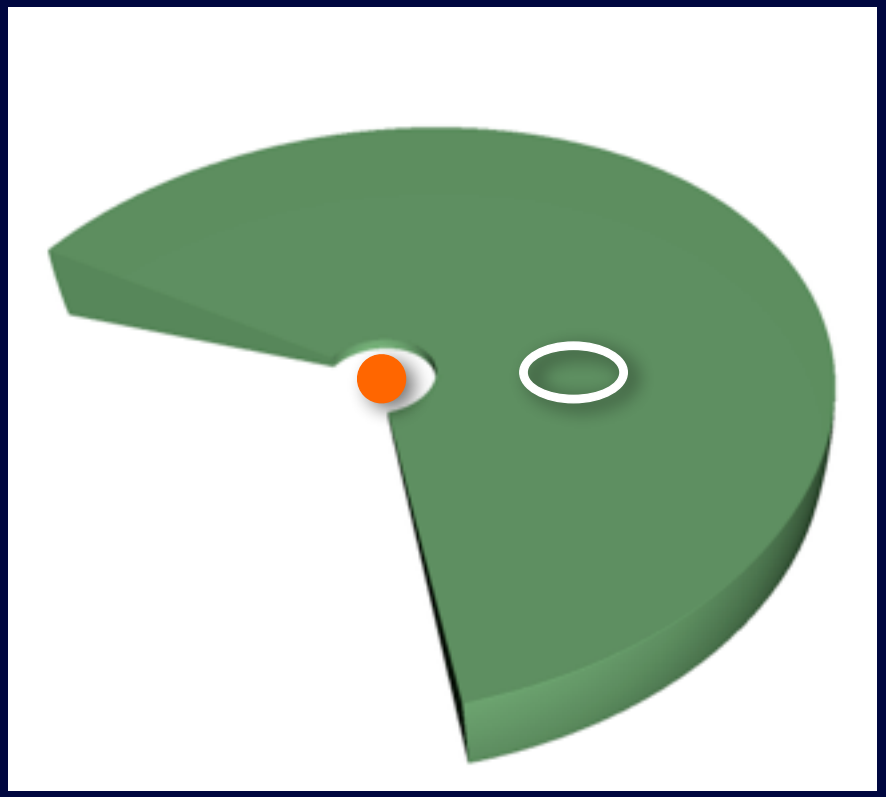

In large wavenumber limit $\omega_{i1} = \omega_{i2} = \omega_s/2$
(Fromang & Papaloizou 2007)

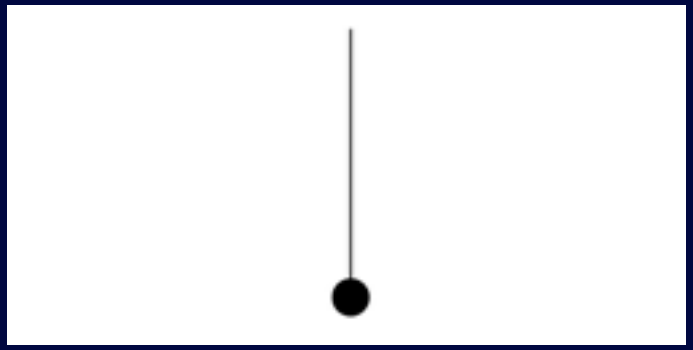

Origin of the instability

- Pairs of inertial modes amplify as they resonantly couple with and extract energy from the background spiral wave
- Maximum growth rate obtained when $\omega_{i1} + \omega_{i2} = \omega_s$ (Goodman 1993).

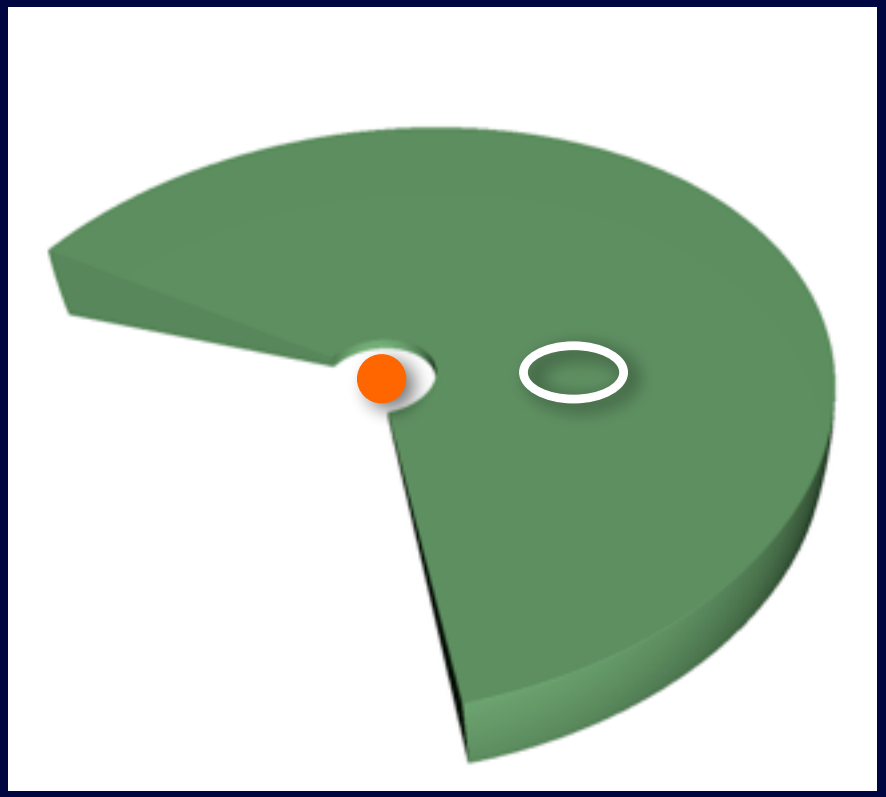

In large wavenumber limit $\omega_{i1} = \omega_{i2} = \omega_s/2$
(Fromang & Papaloizou 2007)

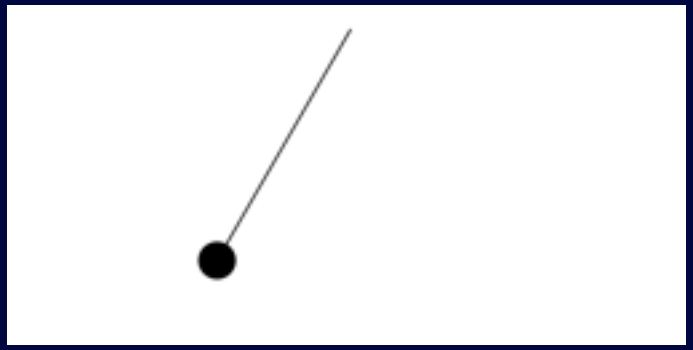

Origin of the instability

- Pairs of inertial modes amplify as they resonantly couple with and extract energy from the background spiral wave
- Maximum growth rate obtained when $\omega_{i1} + \omega_{i2} = \omega_s$ (Goodman 1993).

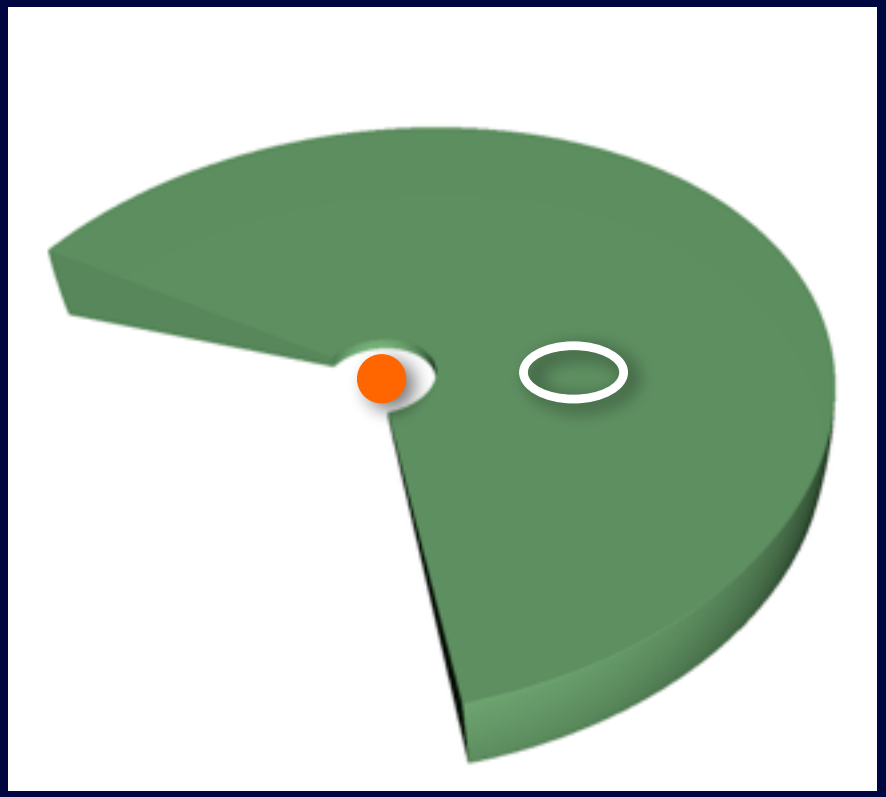

In large wavenumber limit $\omega_{i1} = \omega_{i2} = \omega_s/2$
(Fromang & Papaloizou 2007)

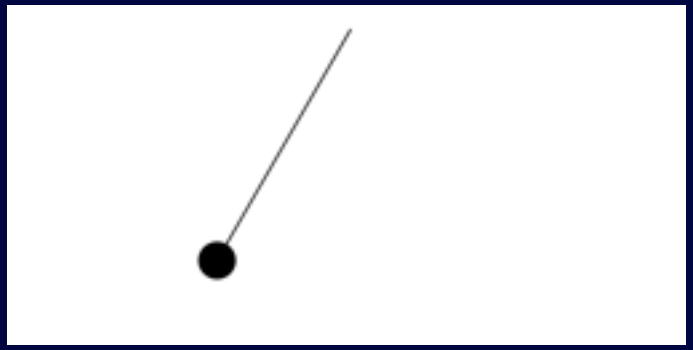

Origin of the instability

- Pairs of inertial modes amplify as they resonantly couple with and extract energy from the background spiral wave
- Maximum growth rate obtained when $\omega_{i1} + \omega_{i2} = \omega_s$ (Goodman 1993).

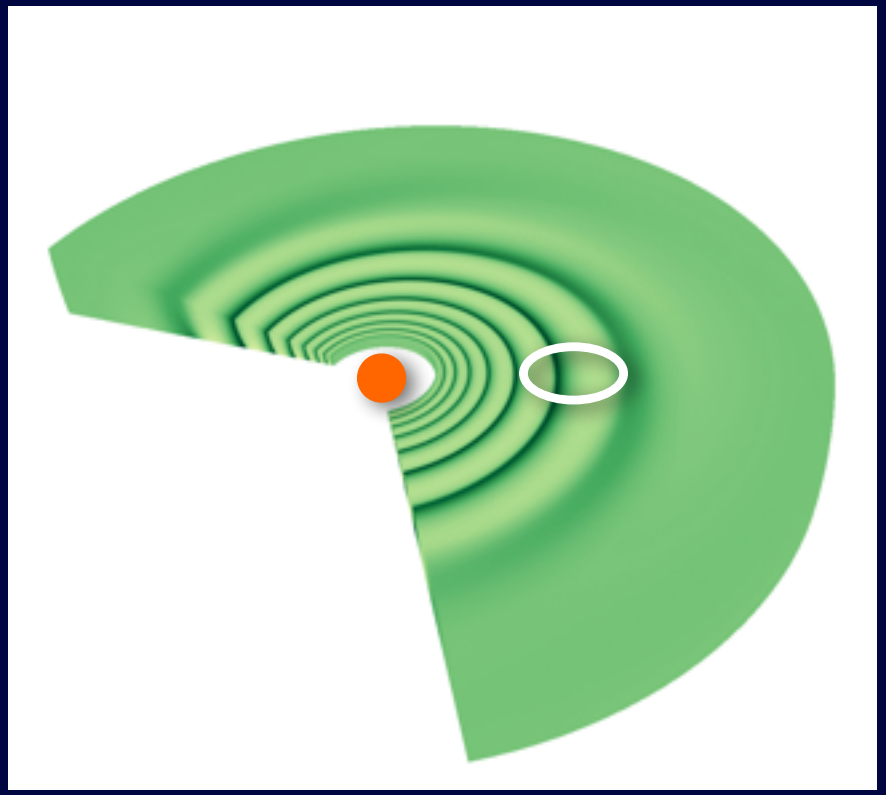

In large wavenumber limit $\omega_{i1} = \omega_{i2} = \omega_s/2$
(Fromang & Papaloizou 2007)

Origin of the instability

- Pairs of inertial modes amplify as they resonantly couple with and extract energy from the background spiral wave
- Maximum growth rate obtained when $\omega_{i1} + \omega_{i2} = \omega_s$ (Goodman 1993).

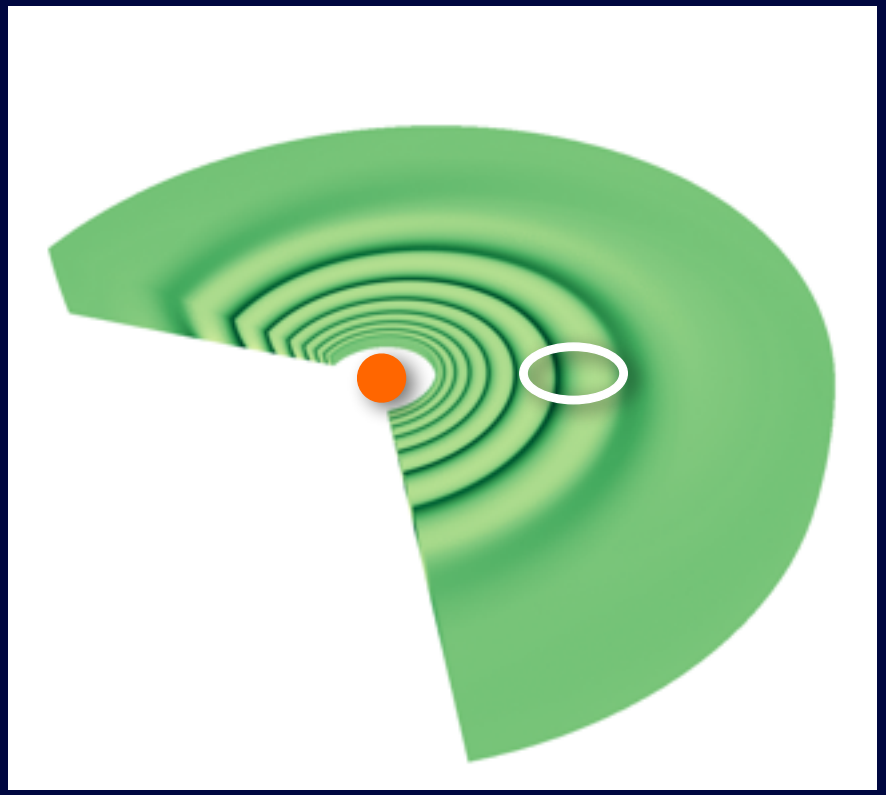

In large wavenumber limit $\omega_{i1} = \omega_{i2} = \omega_s/2$
(Fromang & Papaloizou 2007)

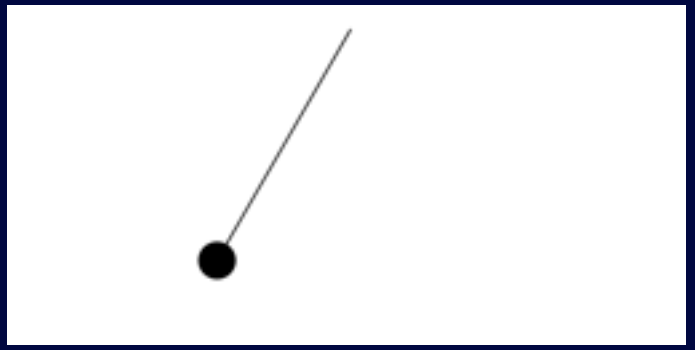

Origin of the instability

- Pairs of inertial modes amplify as they resonantly couple with and extract energy from the background spiral wave
- Maximum growth rate obtained when $\omega_{i1} + \omega_{i2} = \omega_s$ (Goodman 1993).

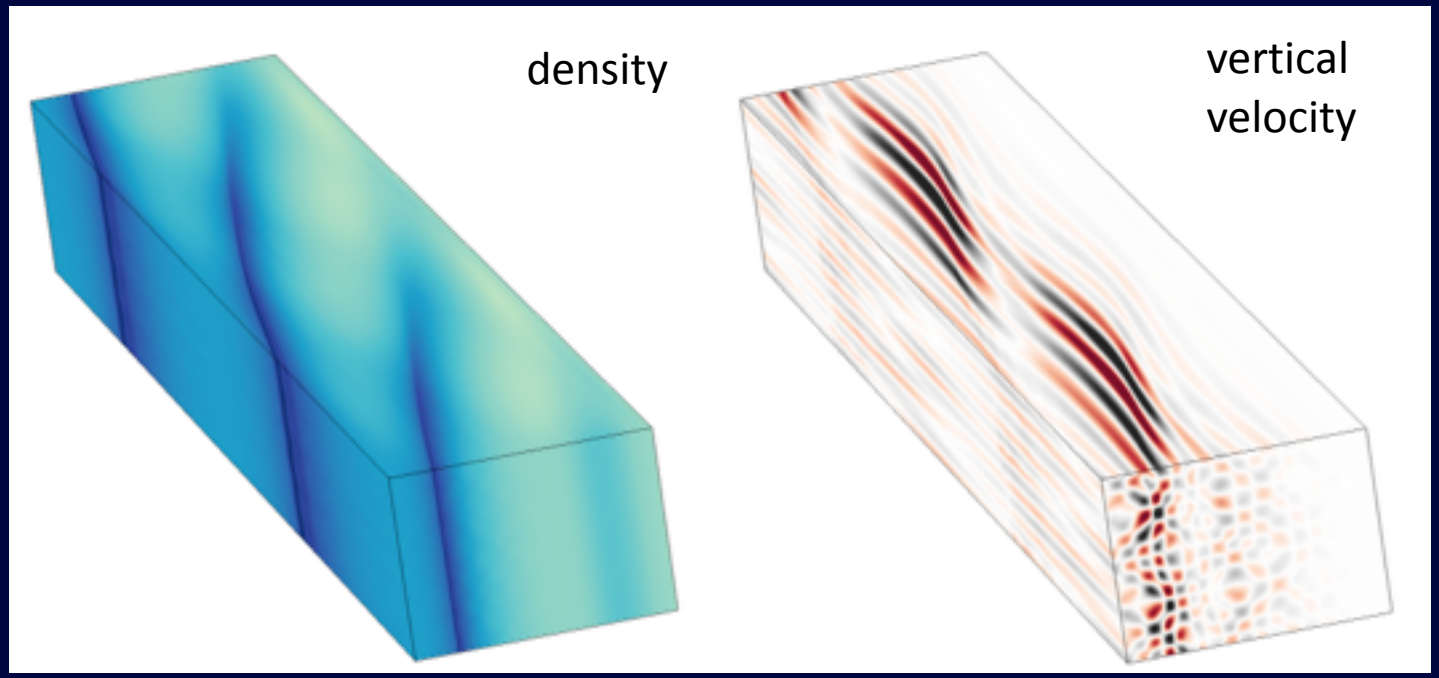

The instability is found to occur

The instability is found to occur

- With various codes (FARGO3D, PLUTO, NIRVANA, …)
- With various numerical resolutions and boundary conditions
- With/without vertical density stratification
- With/without radial temperature gradient
- With different equations of state (isothermal, adiabatic, local cooling)
- With non-zero viscosity (operates with alpha ~ 0.001)
- With imposed monochromatic potentials, planet potentials, binary potentials

Details in Bae et al. 2016a,b and forthcoming work

Vertical Stirring of Solid Particles by Giant Planets

- Place a Jupiter-mass planet in a three-dimensional circumstellar disk ($\Sigma=5\Sigma_{MMSN}$) and estimate vertical stirring of particles due to SWI-induced turbulence

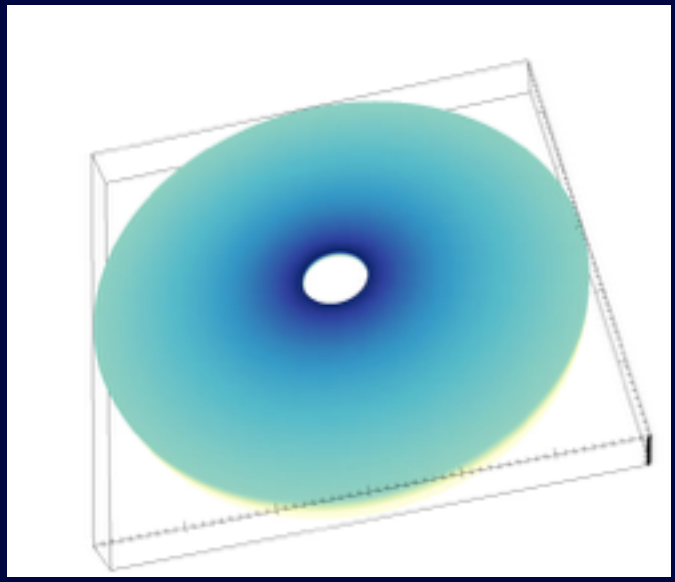

Vertical Stirring of Solid Particles by Giant Planets

- Place a Jupiter-mass planet in a three-dimensional circumstellar disk ($\Sigma=5\Sigma_{MMSN}$) and estimate vertical stirring of particles due to SWI-induced turbulence

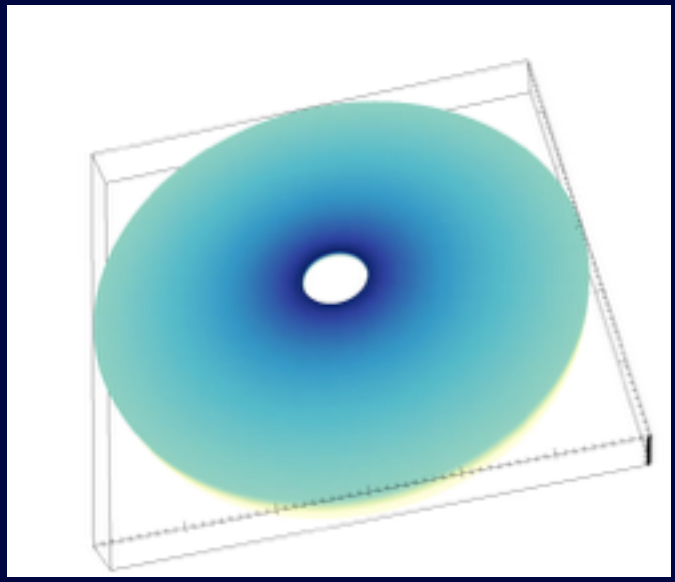

Vertical Stirring of Solid Particles by Giant Planets

- Place a Jupiter-mass planet in a three-dimensional circumstellar disk ($\Sigma=5\Sigma_{MMSN}$) and estimate vertical stirring of particles due to SWI-induced turbulence

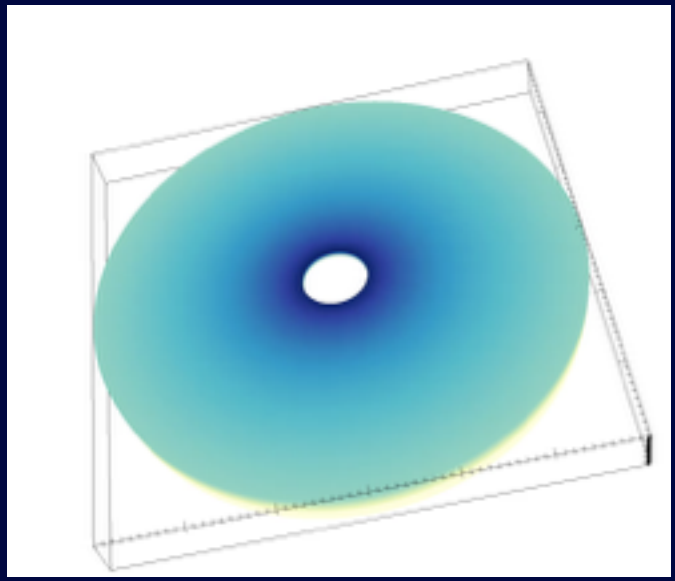

The largest particle sizes that can be vertically dispersed up to one pressure scale height.

Bae et al. (2016c)

TABLE 1
PLANET RUN RESULTS

R	$\langle v_\theta^2 \rangle$	$\langle v_\theta^2 \rangle^{1/2}/\langle c_s \rangle$	t_{corr} (t_{orb})	t_{corr} (Ω^{-1})	$\mathcal{D}_Z$	α_{diff}	t_{mix} (t_{orb})	$\langle \rho_g \rangle$ (g cm^{-3})	$(9/4)\lambda$ (cm)	s_{mix} (cm)
0.3	3.08×10^{-5}	0.050	0.43	2.62	8.32×10^{-5}	0.0065	0.62	8.05×10^{-10}	2.49	4.63
0.4	3.15×10^{-5}	0.059	0.55	2.17	1.09×10^{-4}	0.0075	0.90	4.32×10^{-10}	4.64	3.20
0.5	2.26×10^{-5}	0.055	0.51	1.44	7.24×10^{-5}	0.0043	2.06	3.36×10^{-10}	5.96	1.75
0.6	8.08×10^{-5}	0.112	0.46	0.99	2.34×10^{-4}	0.0124	0.95	2.16×10^{-10}	9.28	3.99
0.7	1.67×10^{-5}	0.054	0.41	0.70	4.30×10^{-5}	0.0020	7.34	2.30×10^{-10}	8.71	0.82

[a] For the quantities in the brackets $\langle\ \rangle$, we average them over azimuth within $|Z| < 1H$.

Vertical Stirring of Solid Particles by Giant Planets

- Place a Jupiter-mass planet in a three-dimensional circumstellar disk ($\Sigma=5\Sigma_{MMSN}$) and estimate vertical stirring of particles due to SWI-induced turbulence

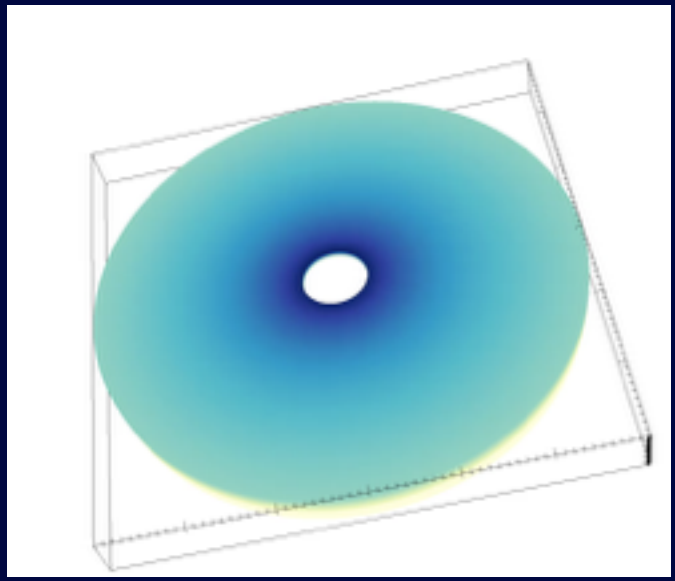

The largest particle sizes that can be vertically dispersed up to one pressure scale height.

Bae et al. (2016c)

TABLE 1
PLANET RUN RESULTS

R	$\langle v_\theta^2 \rangle$	$\langle v_\theta^2 \rangle^{1/2}/\langle c_s \rangle$	t_{corr} (t_{orb})	t_{corr} (Ω^{-1})	$\mathcal{D}_Z$	α_{diff}	t_{mix} (t_{orb})	$\langle \rho_g \rangle$ (g cm^{-3})	$(9/4)\lambda$ (cm)	s_{mix} (cm)
0.3	3.08×10^{-5}	0.050	0.43	2.62	8.32×10^{-5}	0.0065	0.62	8.05×10^{-10}	2.49	4.63
0.4	3.15×10^{-5}	0.059	0.55	2.17	1.09×10^{-4}	0.0075	0.90	4.32×10^{-10}	4.64	3.20
0.5	2.26×10^{-5}	0.055	0.51	1.44	7.24×10^{-5}	0.0043	2.06	3.36×10^{-10}	5.96	1.75
0.6	8.08×10^{-5}	0.112	0.46	0.99	2.34×10^{-4}	0.0124	0.95	2.16×10^{-10}	9.28	3.99
0.7	1.67×10^{-5}	0.054	0.41	0.70	4.30×10^{-5}	0.0020	7.34	2.30×10^{-10}	8.71	0.82

[a] For the quantities in the brackets $\langle\ \rangle$, we average them over azimuth within $|Z| < 1H$.

Gas-drag-aided Pebble Accretion

Johansen & Lacerda 2010, Ormel & Klahr 2010, Lambrechts & Johansen 2012, Morbidelli et al. 2012, …

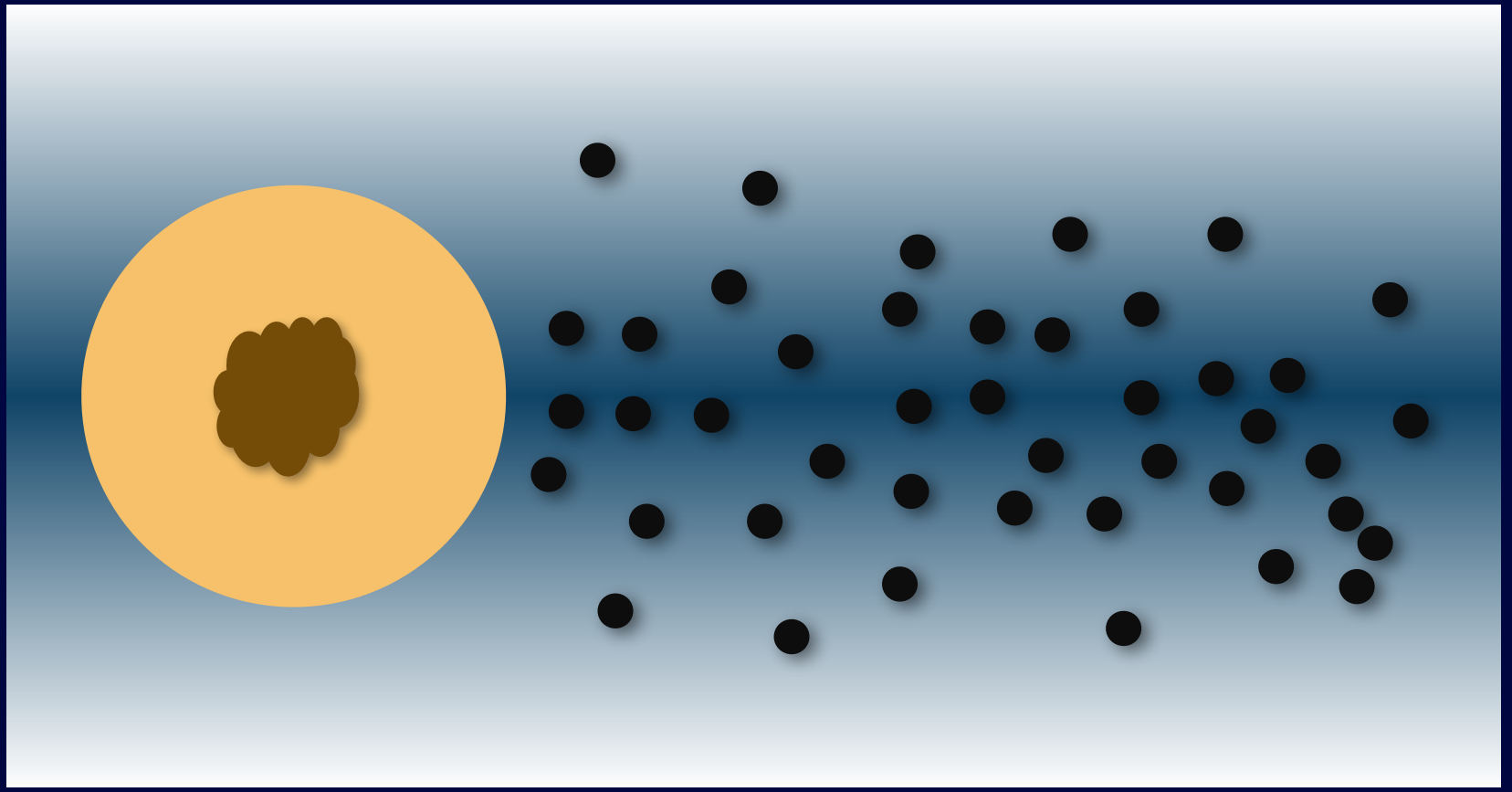

Not to scale!

Gas-drag-aided Pebble Accretion

Johansen & Lacerda 2010, Ormel & Klahr 2010, Lambrechts & Johansen 2012, Morbidelli et al. 2012, …

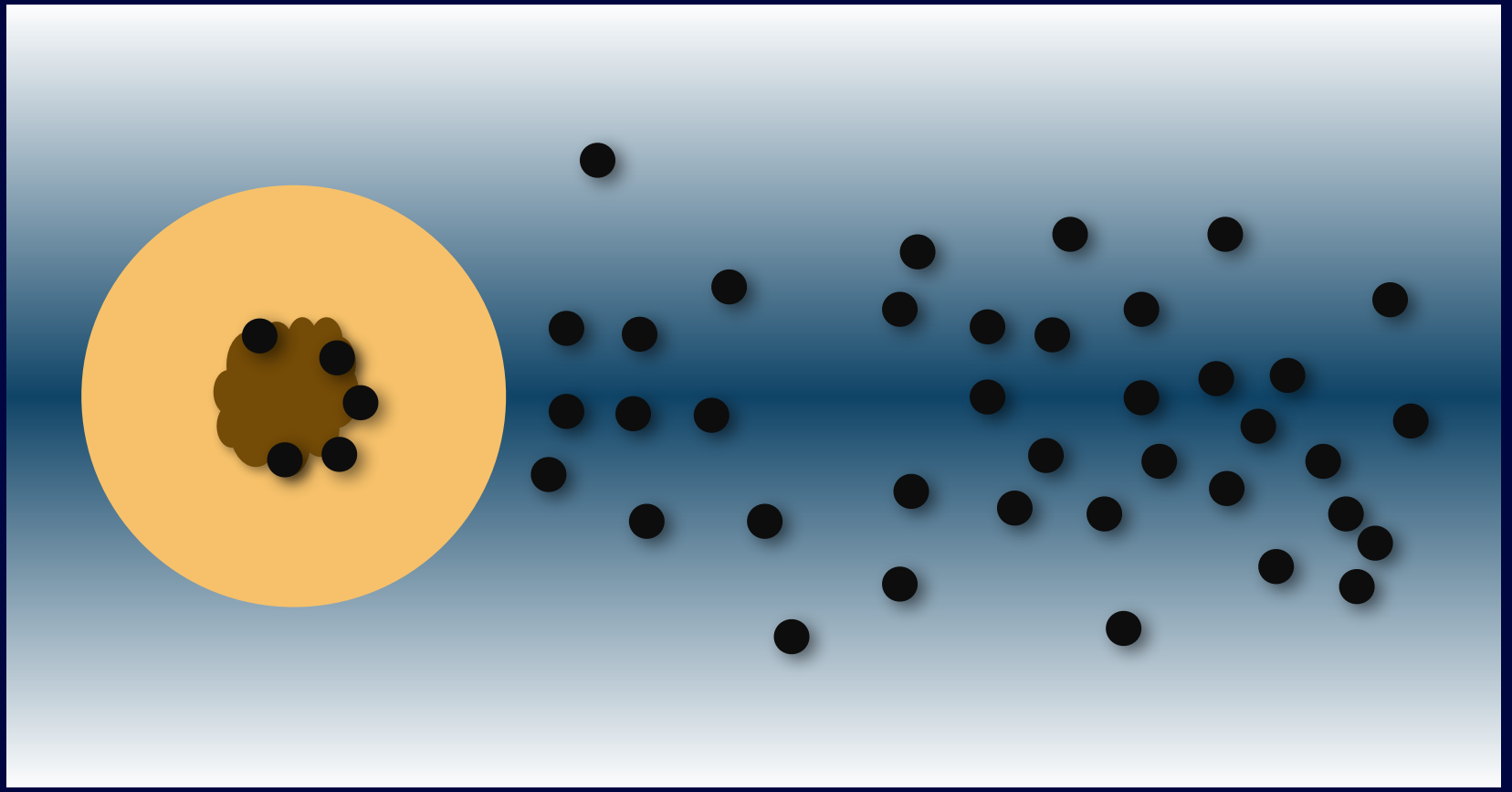

Not to scale!

Gas-drag-aided Pebble Accretion

Johansen & Lacerda 2010, Ormel & Klahr 2010, Lambrechts & Johansen 2012, Morbidelli et al. 2012, …

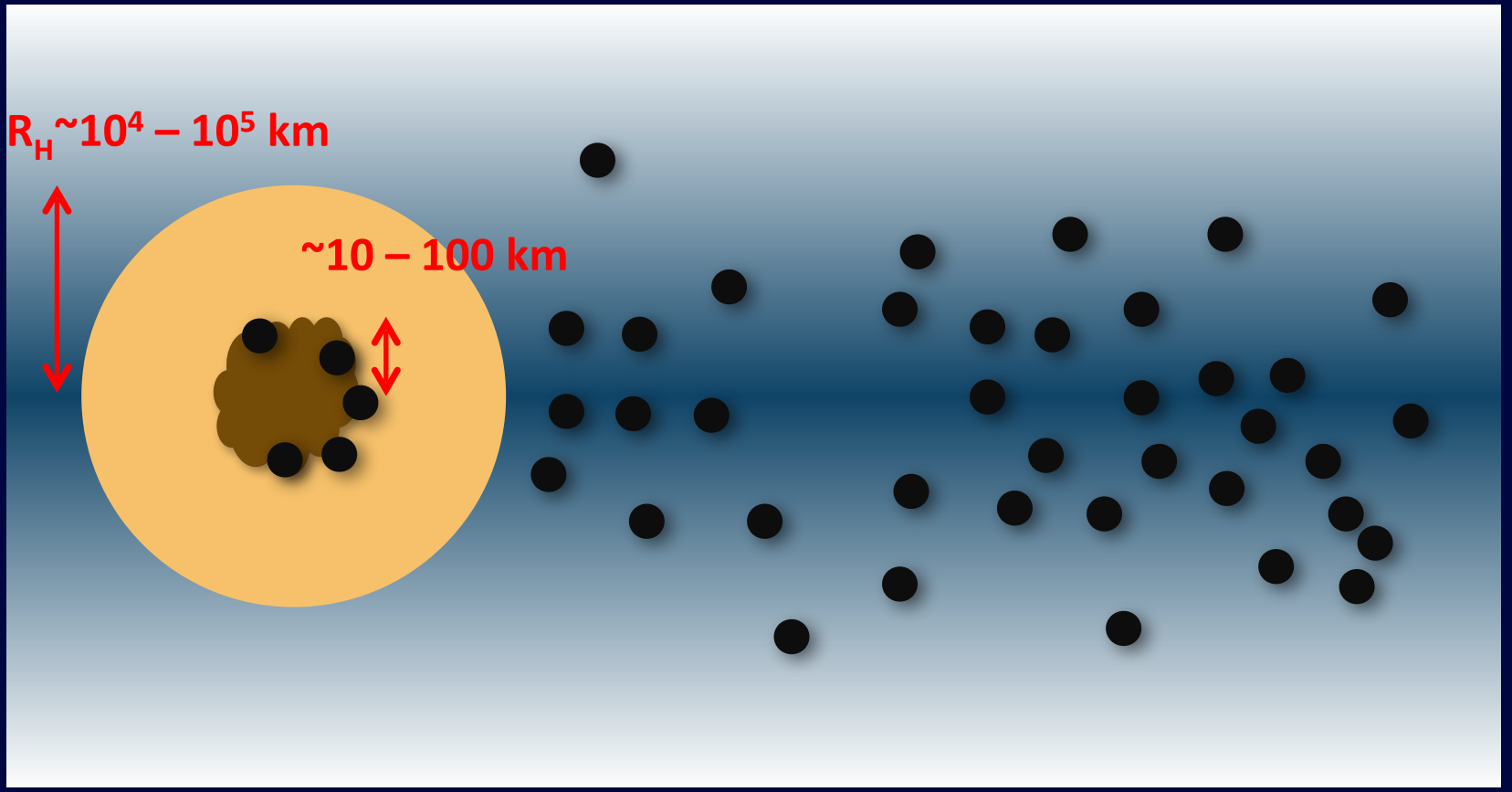

Not to scale!

Gas-drag-aided Pebble Accretion

Johansen & Lacerda 2010, Ormel & Klahr 2010, Lambrechts & Johansen 2012, Morbidelli et al. 2012, …

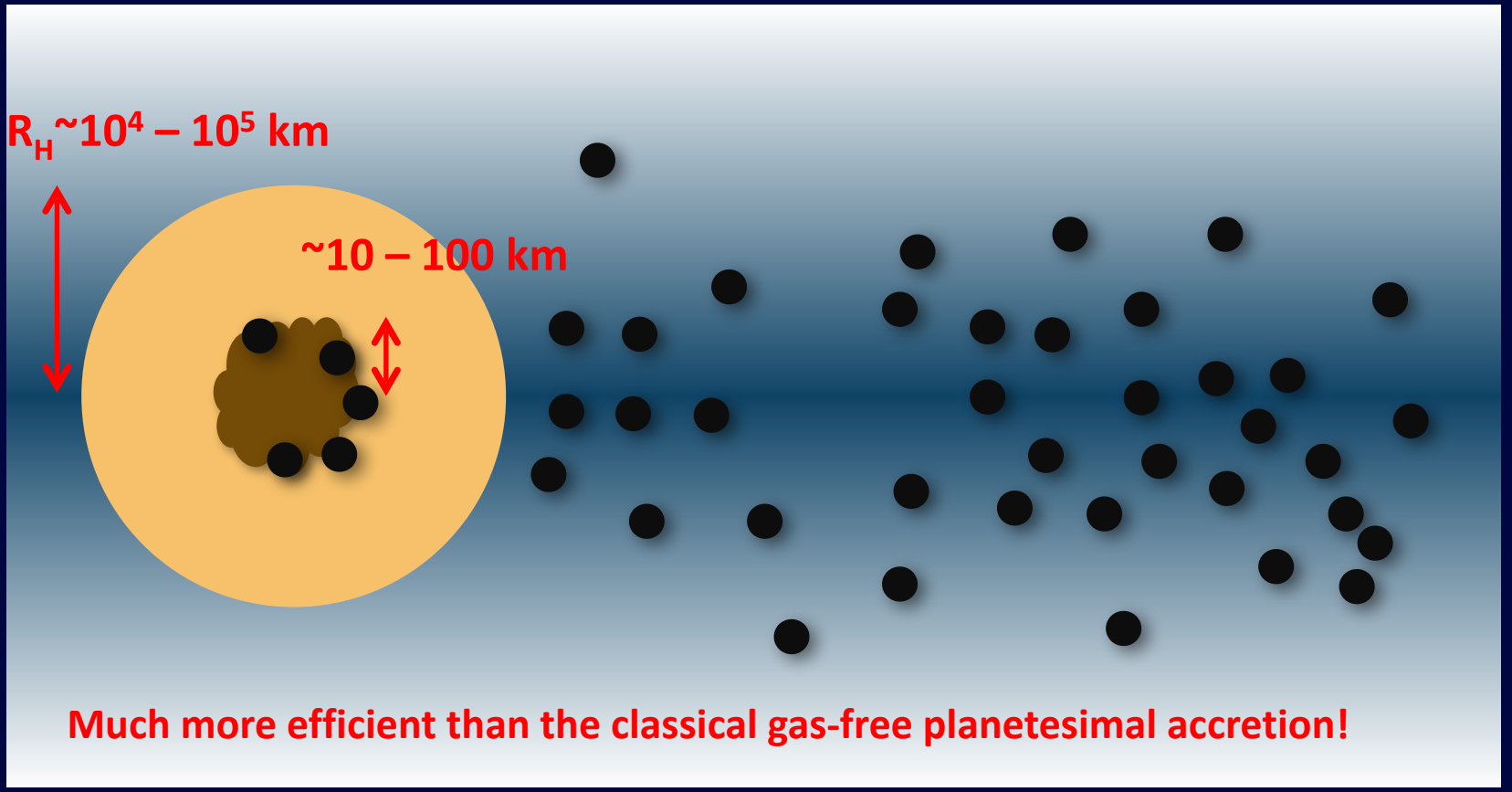

Not to scale!

Gas-drag-aided Pebble Accretion

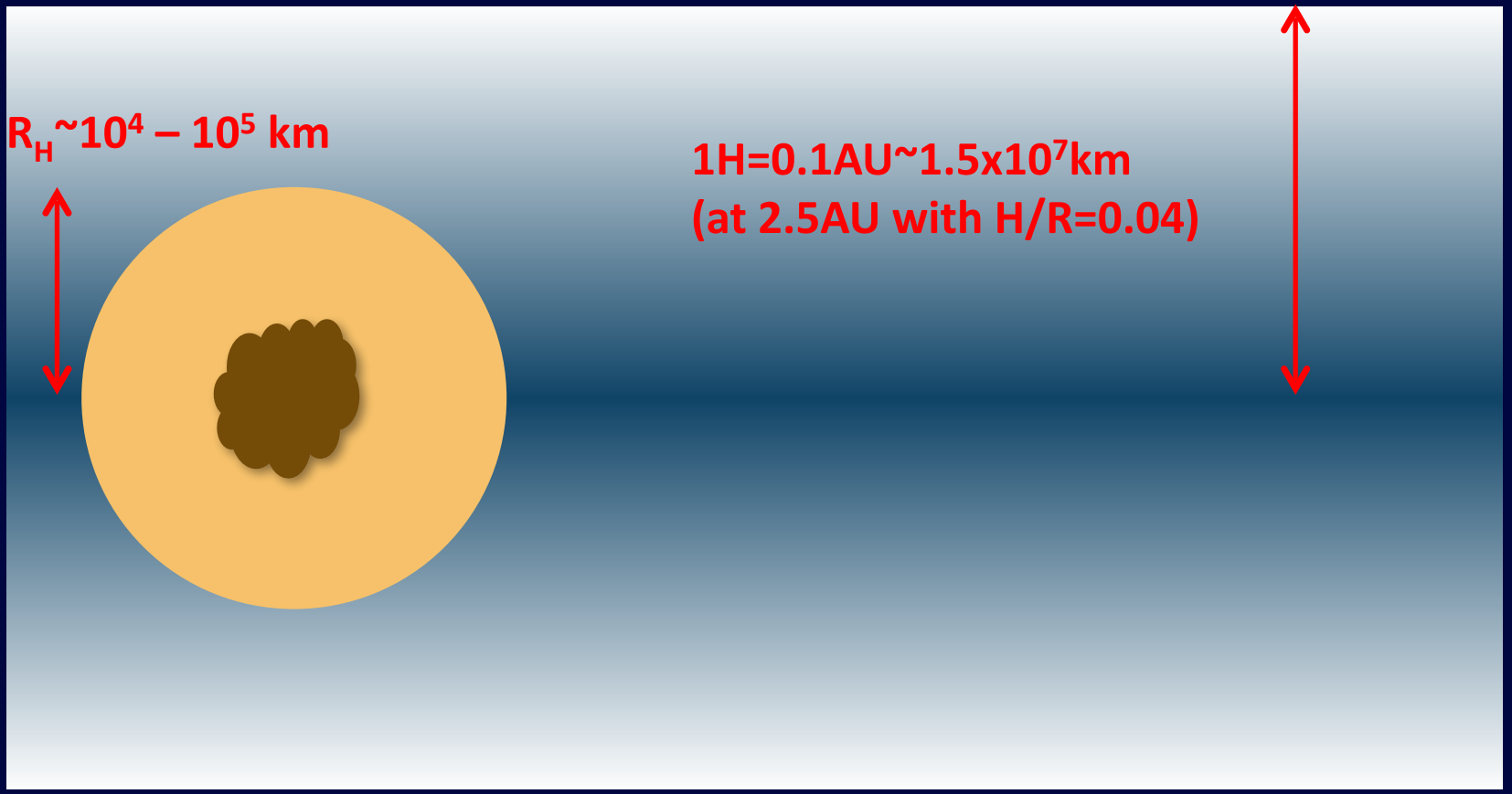

Not to scale!

Gas-drag-aided Pebble Accretion

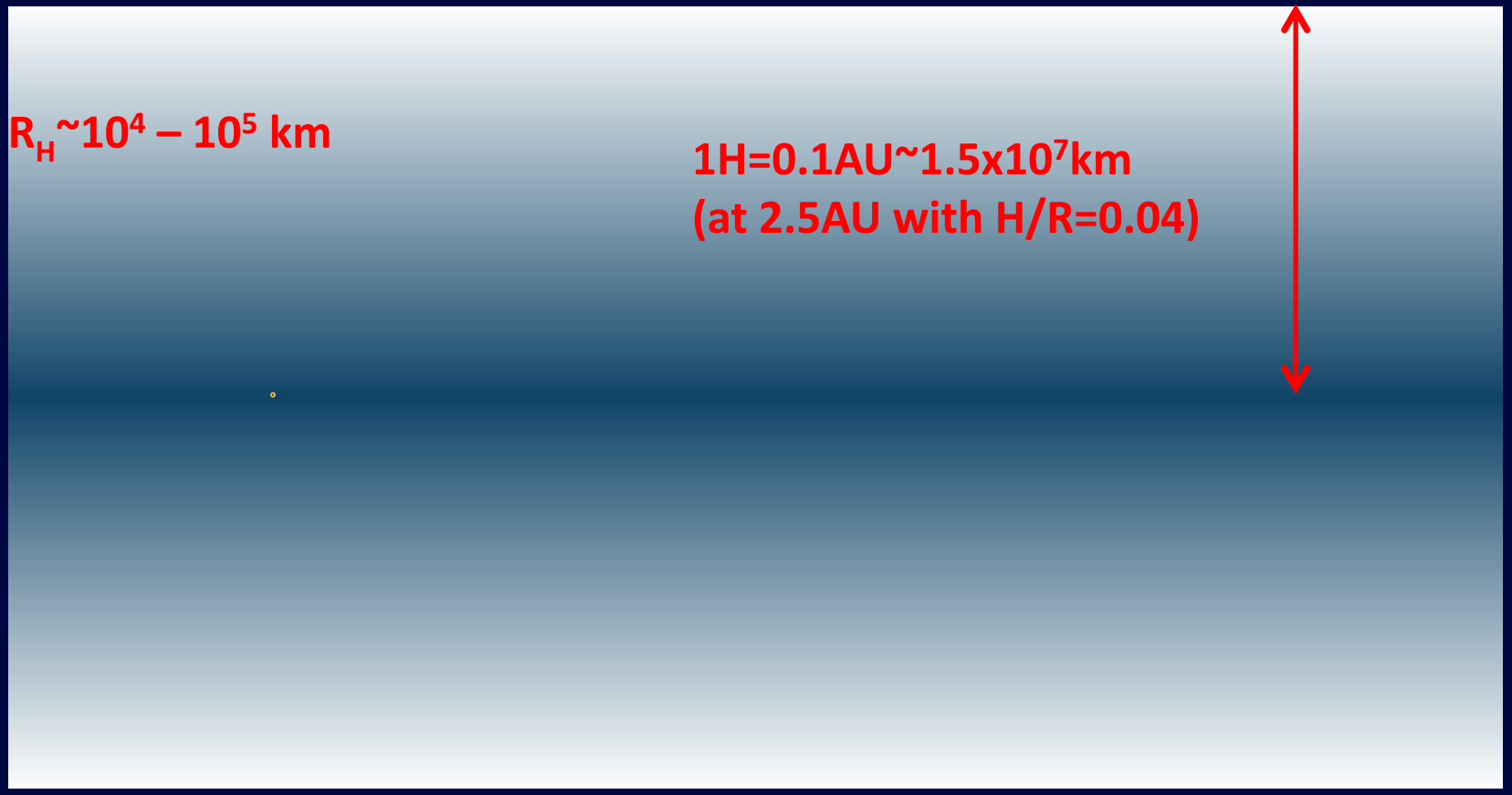

TO SCALE!

Gas-drag-aided Pebble Accretion

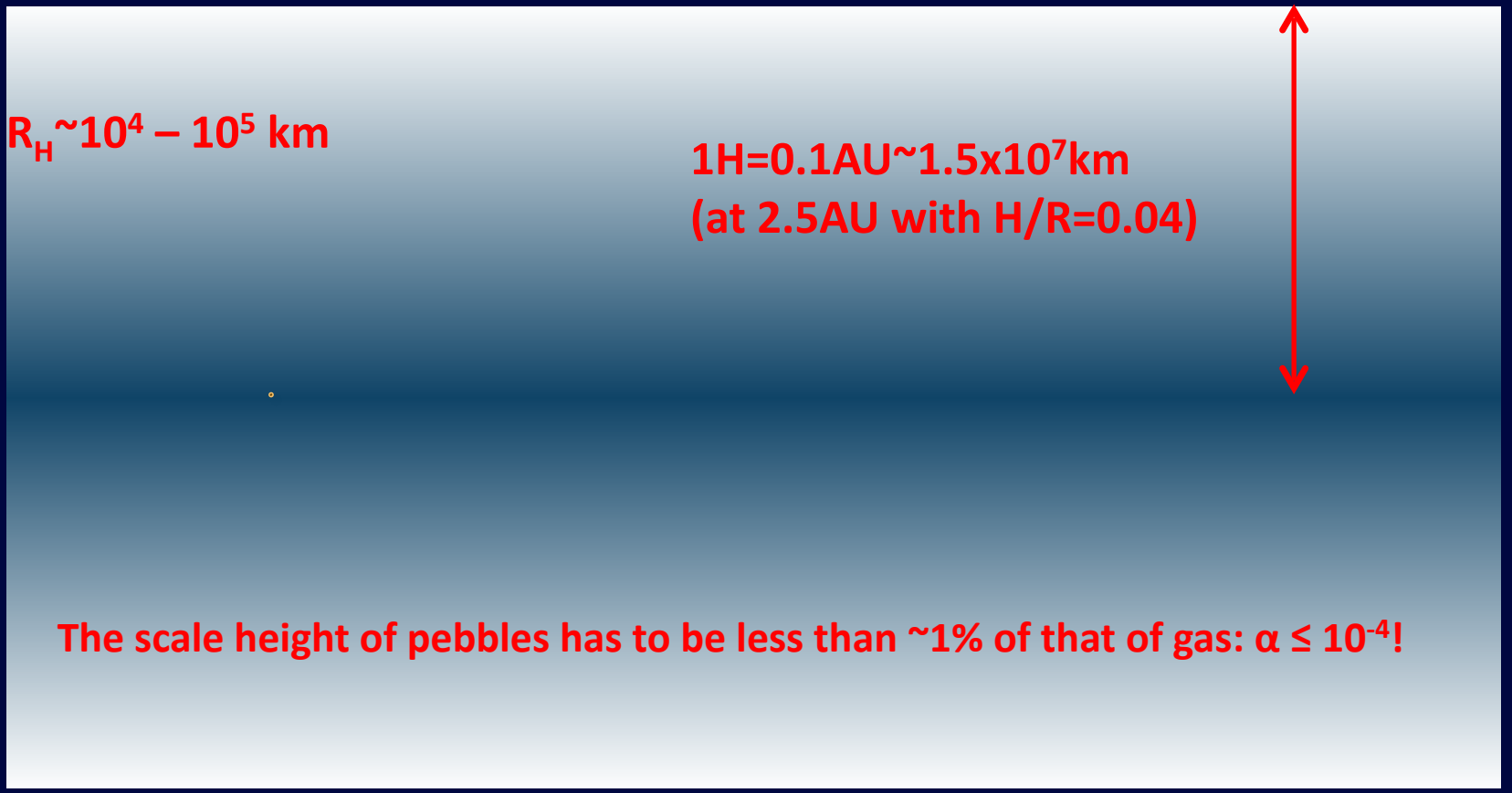

TO SCALE!

Growth of asteroids, planetary embryos, and Kuiper belt objects by chondrule accretion

Anders Johansen,[1]* Mordecai-Mark Mac Low,[2] Pedro Lacerda,[3] Martin Bizzarro[4]

- Planetesimals initially have sizes in a range of 10 – 150km.
- $0.2M_E$ initially in mm-sized particles + $0.2M_E$ continuously added over the next 3Myr.

Growth of asteroids, planetary embryos, and Kuiper belt objects by chondrule accretion

Anders Johansen,[1]* Mordecai-Mark Mac Low,[2] Pedro Lacerda,[3] Martin Bizzarro[4]

- Planetesimals initially have sizes in a range of 10 – 150km.
- $0.2M_E$ initially in mm-sized particles + $0.2M_E$ continuously added over the next 3Myr.

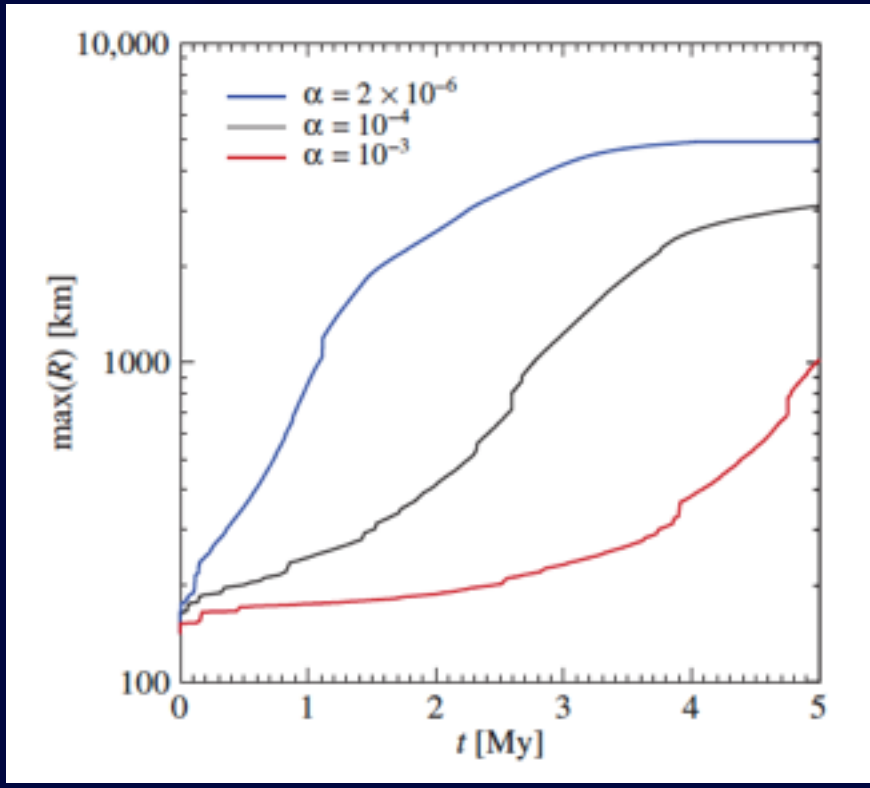

Growth of asteroids, planetary embryos, and Kuiper belt objects by chondrule accretion

Anders Johansen,[1]* Mordecai-Mark Mac Low,[2] Pedro Lacerda,[3] Martin Bizzarro[4]

- Planetesimals initially have sizes in a range of 10 – 150km.
- $0.2M_E$ initially in mm-sized particles + $0.2M_E$ continuously added over the next 3Myr.

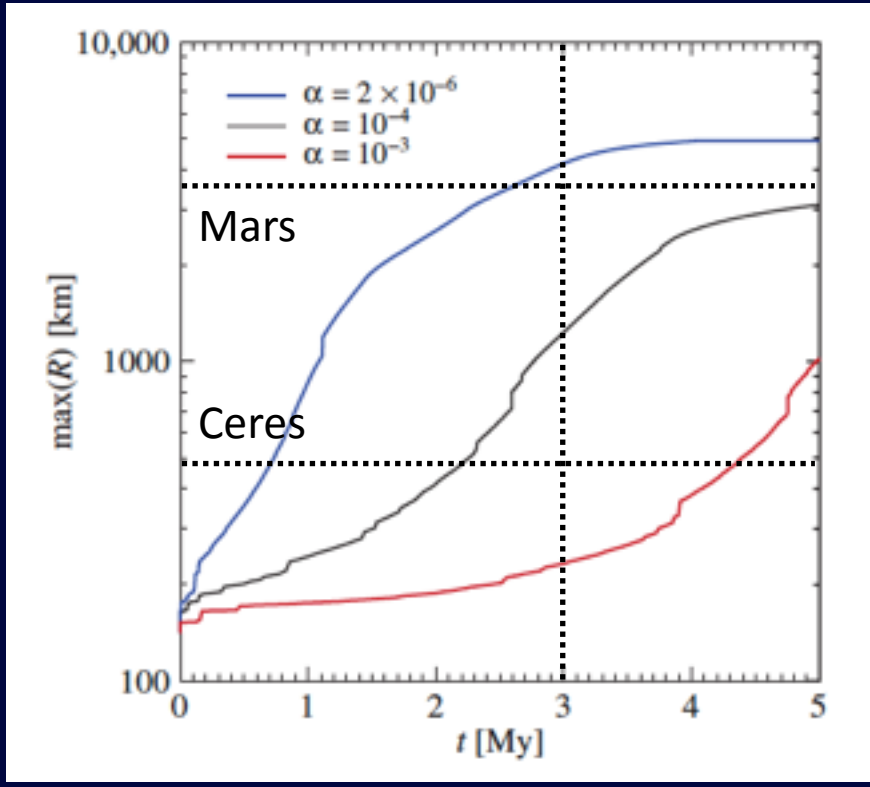

Growth of asteroids, planetary embryos, and Kuiper belt objects by chondrule accretion

Anders Johansen,[1]* Mordecai-Mark Mac Low,[2] Pedro Lacerda,[3] Martin Bizzarro[4]

- Planetesimals initially have sizes in a range of 10 – 150km.
- $0.2M_E$ initially in mm-sized particles + $0.2M_E$ continuously added over the next 3Myr.

$\alpha_{\rm diff}$
0.0065
0.0075
0.0043
0.0124
0.0020

Bae et al. (2016b)

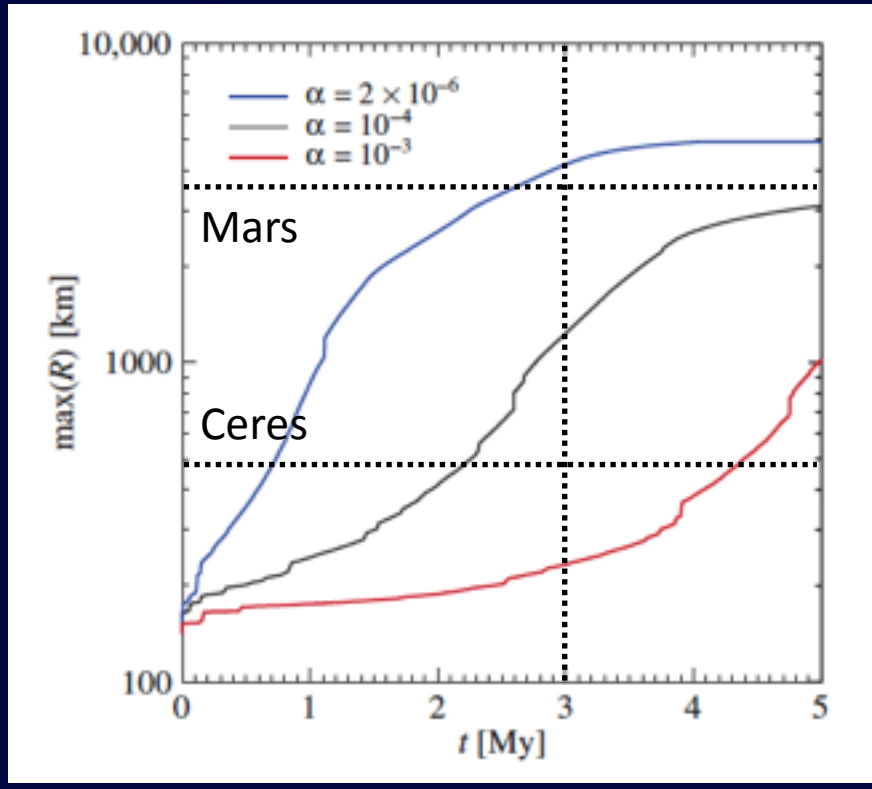

Growth of asteroids, planetary embryos, and Kuiper belt objects by chondrule accretion

Anders Johansen,[1]* Mordecai-Mark Mac Low,[2] Pedro Lacerda,[3] Martin Bizzarro[4]

- Planetesimals initially have sizes in a range of 10 – 150km.
- $0.2M_E$ initially in mm-sized particles + $0.2M_E$ continuously added over the next 3Myr.

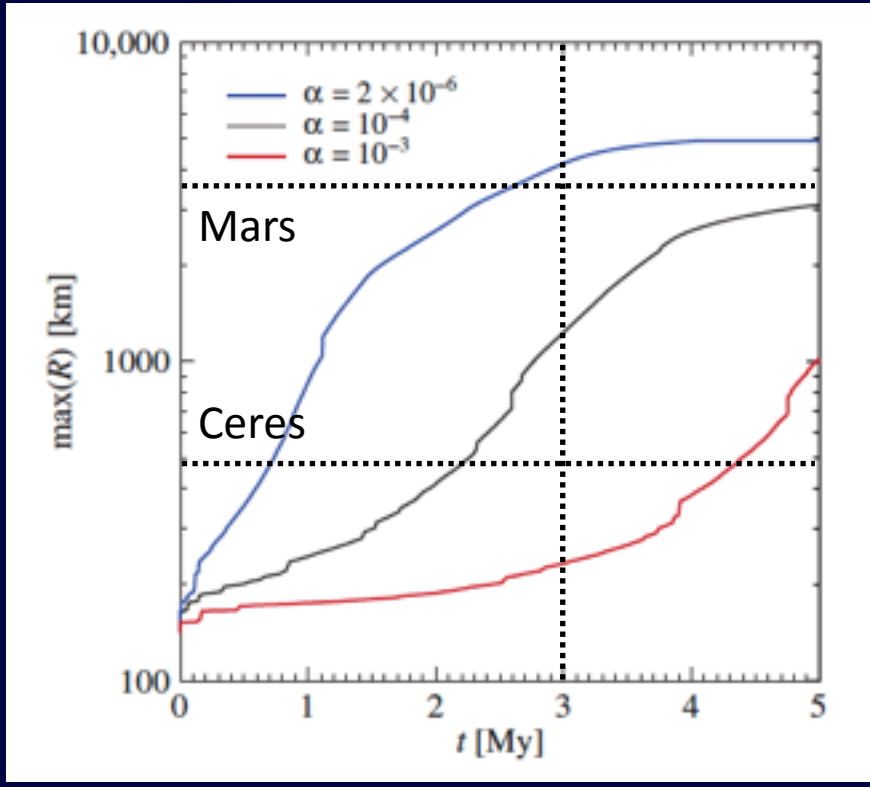

Growth of asteroids, planetary embryos, and Kuiper belt objects by chondrule accretion

Anders Johansen,[1]* Mordecai-Mark Mac Low,[2] Pedro Lacerda,[3] Martin Bizzarro[4]

- Planetesimals initially have sizes in a range of 10 – 150km.
- $0.2M_E$ initially in mm-sized particles + $0.2M_E$ continuously added over the next 3Myr.

- This does NOT disprove pebble accretion!
- The SWI can help better understand the timing of planetary body formation.

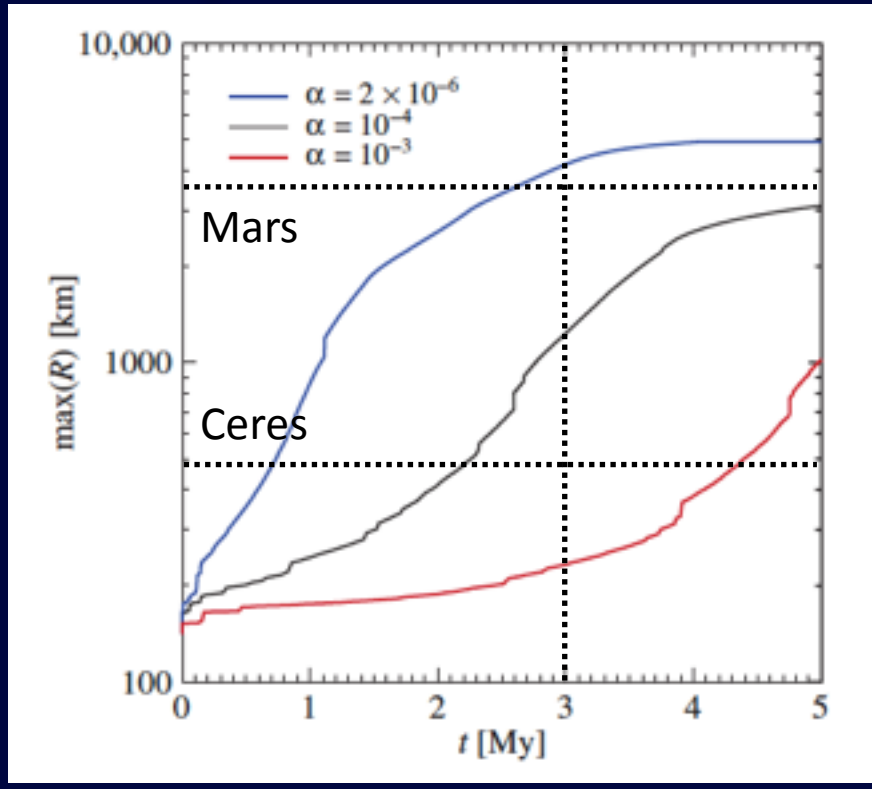

Growth of asteroids, planetary embryos, and Kuiper belt objects by chondrule accretion

Anders Johansen,[1]* Mordecai-Mark Mac Low,[2] Pedro Lacerda,[3] Martin Bizzarro[4]

- Planetesimals initially have sizes in a range of 10 – 150km.
- $0.2M_E$ initially in mm-sized particles + $0.2M_E$ continuously added over the next 3Myr.

- This does NOT disprove pebble accretion!
- The SWI can help better understand the timing of planetary body formation.
- The early formation scenario of Mars is consistent of the isotope measurement of Martian meteorites

(Dauphas & Pourmand 2011).

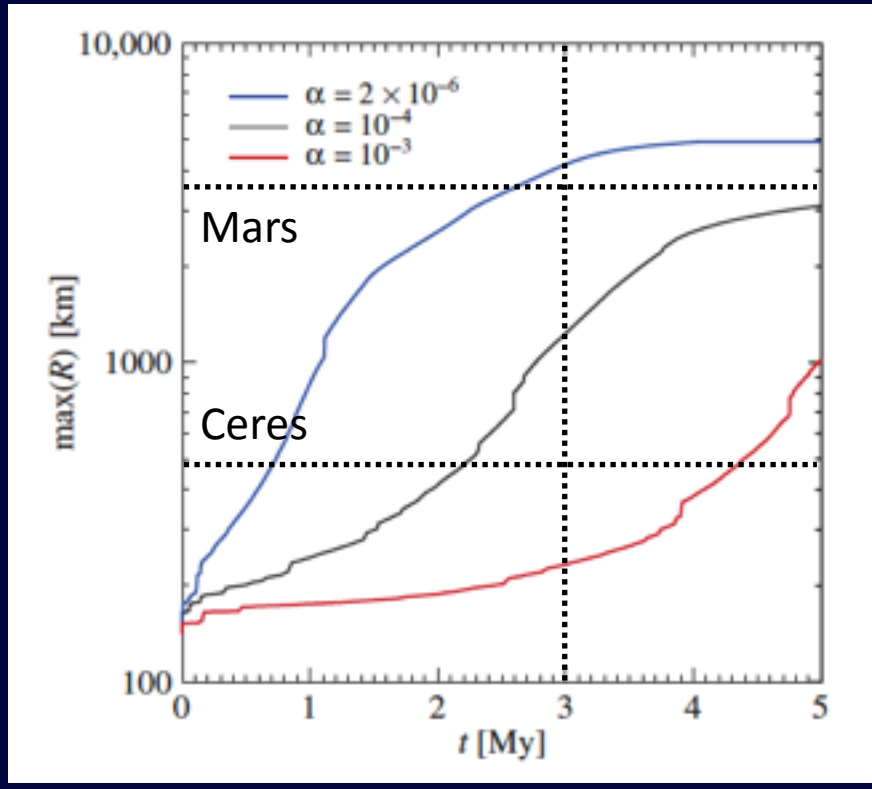

Observability of SWI in scattered light

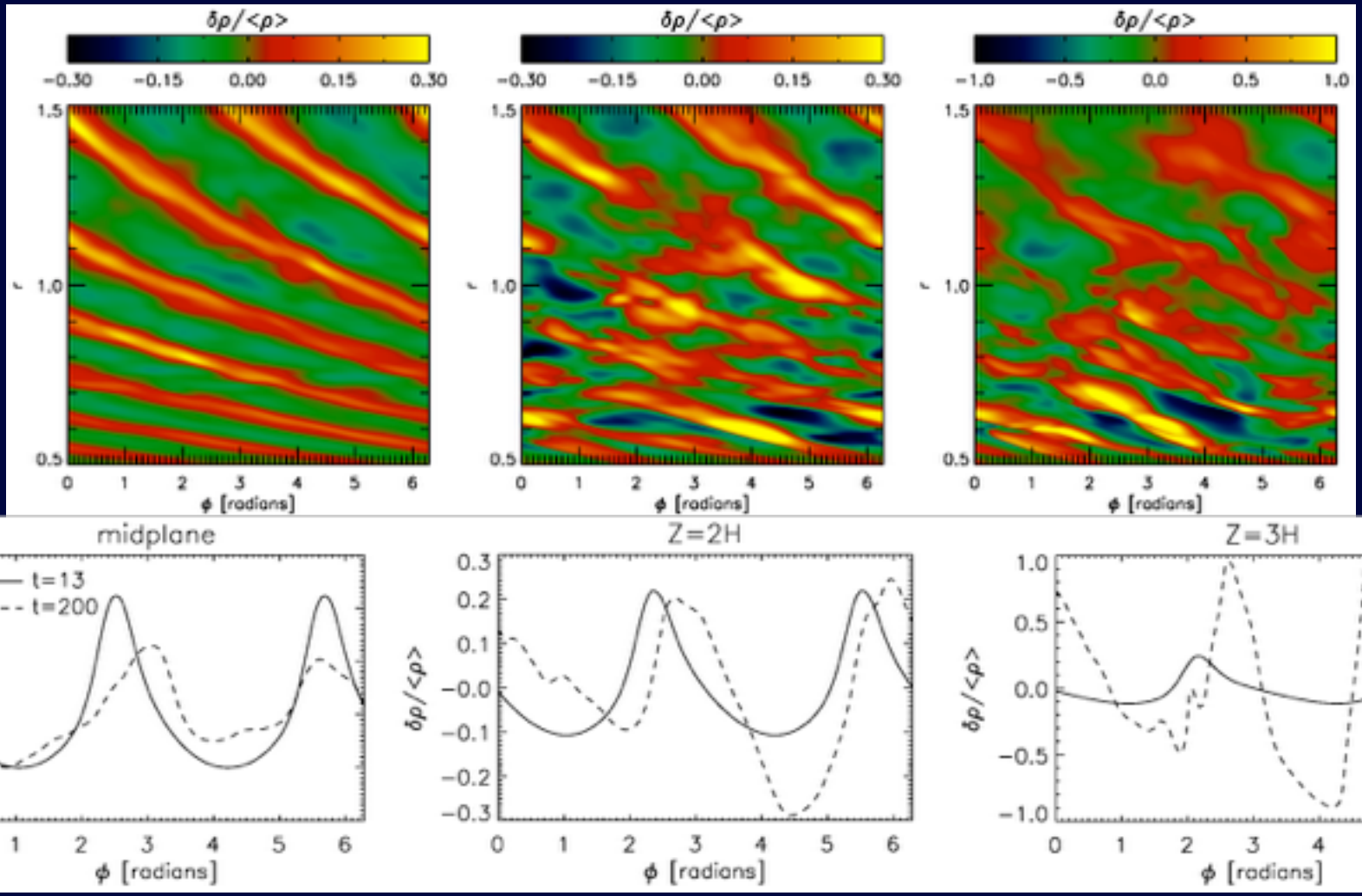

Bae et al. (2016a)

Observability of SWI in scattered light

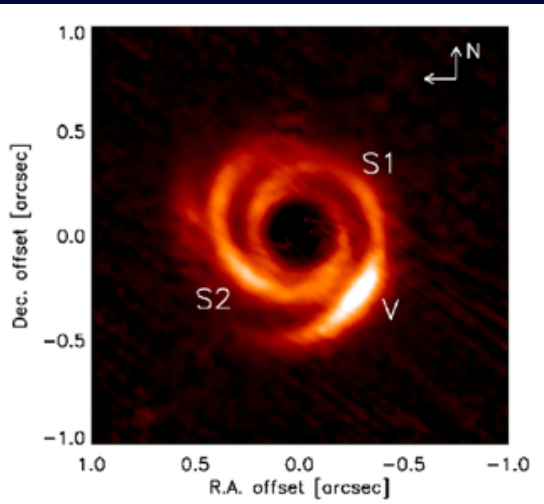

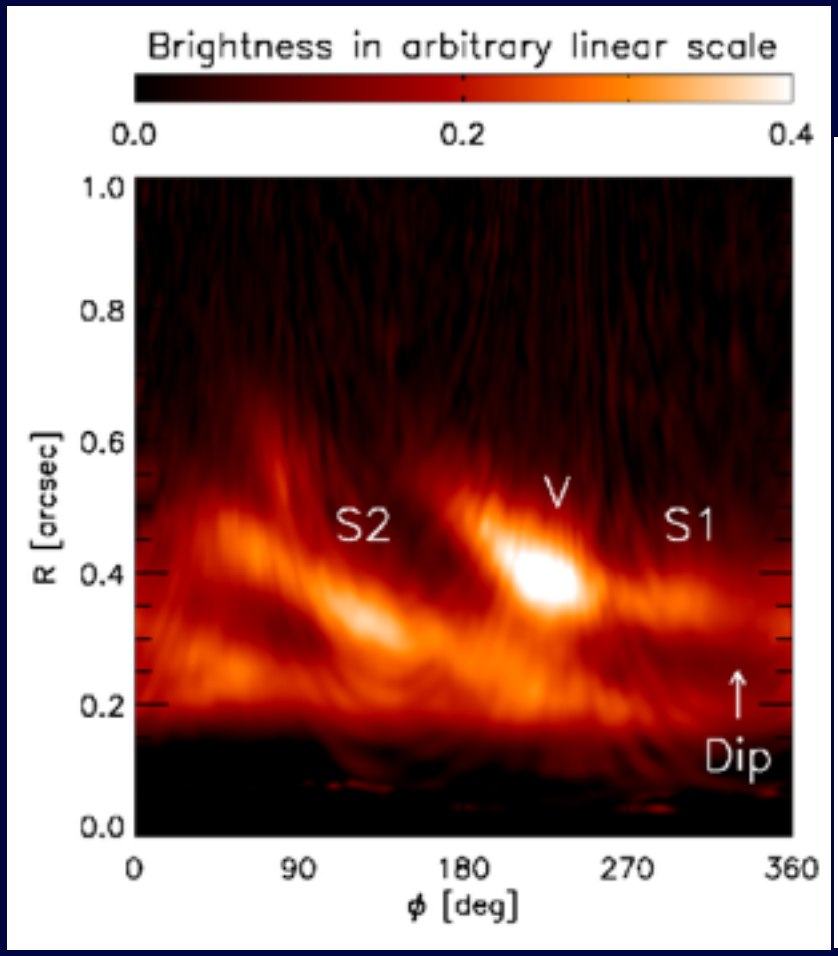

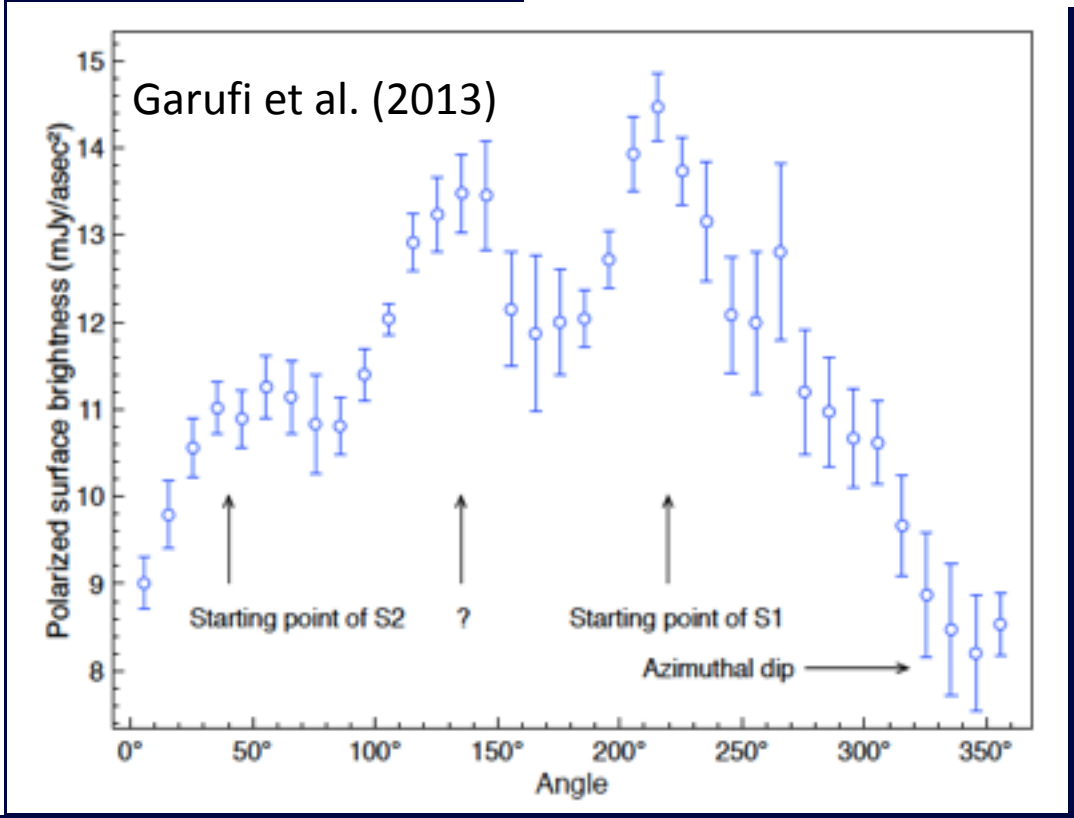

Summary

- VSI may operate in outer regions of protoplanetary discs
  - induce turbulence with $v_{turb} \sim 0.2 \times c_s$ and stir solid particles
  - need to examine in presence of magnetic fields and non-ideal MHD
- SWI leads to significant modification of spiral wave amplitudes and morphologies
- Giant planets can induce turbulence that significantly stirs up solid particles and thus can affect
  - the subsequent planet formation in the disk and
  - the appearance of the disc
- Role of SWI in planet formation in binaries and in FU Orionis outbursts currently under investigation…